

Tunable Domain Adaptation Using Unfolding

Snehaa Reddy*, Jayaprakash Katual*, and Satish Mulleti, *Member, IEEE*

Abstract—Machine learning models often struggle to generalize across domains with varying data distributions, such as differing noise levels, leading to degraded performance. Traditional strategies like personalized training, which trains separate models per domain, and joint training, which uses a single model for all domains, have significant limitations in flexibility and effectiveness. To address this, we propose two novel domain adaptation methods for regression tasks based on interpretable unrolled networks—deep architectures inspired by iterative optimization algorithms. These models leverage the functional dependence of select tunable parameters on domain variables, enabling controlled adaptation during inference. Our methods include Parametric Tunable-Domain Adaptation (P-TDA), which uses known domain parameters for dynamic tuning, and Data-Driven Tunable-Domain Adaptation (DD-TDA), which infers domain adaptation directly from input data. We validate our approach on compressed sensing problems involving noise-adaptive sparse signal recovery, domain-adaptive gain calibration, and domain-adaptive phase retrieval, demonstrating improved or comparable performance to domain-specific models while surpassing joint training baselines. This work highlights the potential of unrolled networks for effective, interpretable domain adaptation in regression settings.

Index Terms—Unfolding, domain-adaptation, model-based learning, compressive sensing, blind-gain calibration.

I. INTRODUCTION

MACHINE learning models typically learn input-output mappings by optimizing parameters to minimize prediction errors on paired data. Their ability to generalize effectively to unseen data hinges on the assumption that both training and test data are drawn from similar distributions. However, this assumption often breaks down when data varies due to domain-specific factors, such as noise levels or sensor characteristics, leading to performance degradation. To ensure robust model performance in such settings, it becomes critical to account for this variability during training.

A straightforward strategy to handle domain shifts is *Personalized Training (PT)*, where separate models are trained for each domain. While this yields strong performance, it becomes impractical when the domain parameters vary continuously, and it also requires precise domain information during inference. On the other hand, *Joint Training (JT)* consolidates data from all domains into a single model, eliminating the need for domain-specific information. However, JT typically underperforms compared to PT, as it attempts to learn a unified representation across varying domains, which may not capture domain-specific nuances effectively.

To address the issues arising in the PT and JT approaches, *transfer learning* and *domain adaptation* techniques have been proposed, often outperforming both PT and JT. In classification tasks, these methods commonly involve retraining only the final layers of a model, under the assumption that the feature extractor is domain-invariant [1], [2], [3], [4]. However, identifying which layers should serve as feature extractors is non-trivial [5]. In [6], the authors describe a gradual domain adaptation method using optimal transport to improve classification performance across large domain shifts. In [7], Farhani *et al.* describe domain adaptation methods that address domain shifts by aligning features between domains, learning deep domain-invariant representations, iteratively refining models with pseudo-labels on target data, and using adversarial training to make features indistinguishable across domains. These require separate domain-specific data for progressive retraining during adaptation. However, these approaches do not extend naturally to regression tasks—particularly to those with parametric domain variations—which form the focus of this work [8], [9], [10], [11].

Our goal is to develop domain adaptation methods suitable for regression problems where the underlying domains are parameterized by physical or statistical quantities. While Deep Neural Networks (DNNs) and Convolutional Neural Networks (CNNs) have demonstrated strong performance, their non-interpretable nature obscures how internal parameters relate to domain variations, making it difficult to identify which parts of the model should adapt.

In this paper, we address these limitations by adopting *interpretable unrolled networks* [12]—deep learning architectures derived by unfolding iterative optimization algorithms into finite-layer neural networks. These models retain the transparency of classical optimization while benefiting from data-driven learning, making them well-suited for analyzing parameter dependencies. When trained across data with domain variability, the learnable parameters of such networks often exhibit structured dependence on domain-specific factors. Importantly, only a subset of these parameters—termed *tunable parameters*—show systematic variation across domains, while others remain largely invariant. This property enables the modeling of domain effects through a small number of interpretable, low-complexity tuning functions, avoiding extensive retraining.

With the objective of developing a single interpretable network that can adapt efficiently across multiple domains, we introduce two lightweight domain adaptation mechanisms:

- *Parametric Tunable-Domain Adaptation (P-TDA)*: This approach assumes that domain parameters are either known for each data instance or that a simple parametric mapping exists between domain parameters and the tunable parameters of the unrolled network. The model learns this relationship during training and adjusts its in-

* Equal Contribution

The authors are with the Department of Electrical Engineering, Indian Institute of Technology Bombay, Mumbai, India.
Emails: snehaareddy192@gmail.com, kataljayaprakash@gmail.com, mulleti.satish@gmail.com

Codes are available in: <https://github.com/Jay5119/TDA-Unfolding.git>

ternal parameters accordingly during inference, enabling structured adaptation without retraining.

- *Data-Driven Tunable-Domain Adaptation (DD-TDA)*: When explicit domain parameters are unavailable, this approach employs a lightweight function h_φ that infers the relevant domain-dependent quantities directly from the input data. The network then adapts its tunable parameters based on these inferred quantities. This design maintains interpretability while ensuring that additional computational cost remains minimal.

We demonstrate the utility of the proposed framework through three representative *inverse problems*, encompassing both linear and non-linear settings that are commonly encountered in signal recovery and estimation. The first two are closely related to regression problems formulated as inverse tasks in *Compressed Sensing (CS)* [13], and the third one is on phase retrieval, as detailed next.

- *Noise-Adaptive LISTA*: The first application addresses sparse signal recovery under varying noise conditions. The Iterative Shrinkage-Thresholding Algorithm (ISTA) [14] is a well-established iterative solver for sparse recovery, and its learned variant, Learned-ISTA (LISTA) [15], models each ISTA iteration as a distinct network layer, combining interpretability with the expressive power of deep learning. Prior work [16] has shown a strong relationship between the noise standard deviation and the soft-thresholding parameter in LISTA. Here, the *domain parameter* is the noise standard deviation, and the *tunable parameter* is the soft-thresholding coefficient. P-TDA leverages known noise levels to tune the threshold dynamically, while DD-TDA learns to infer this relationship directly from data. Both approaches achieve robust recovery across noise levels with minimal additional parameters.
- *Domain-Adaptive Gain Calibration*: The second application considers a compressed sensing problem involving multiplicative distortions modeled as unknown sensor gains. The domain variability arises from changes in gain. Using explicit gain information (P-TDA) or inferring it from data (DD-TDA), we show that both approaches effectively compensate for gain-induced variability while remaining efficient in parameter count and FLOPs.
- *Domain-Adaptive Phase Retrieval*: The third application extends the framework to the non-linear problem of sparse phase retrieval, where only magnitude measurements are available. Here, the domain parameter is the sparsity level, which directly affects recovery performance but is typically unknown. In the P-TDA setting, the true sparsity is used for adaptation, whereas in DD-TDA, a lightweight sparsity estimation module infers it from measurements. The results demonstrate that both approaches generalize effectively across domains, highlighting the flexibility of the proposed framework in handling non-linear inverse problems.

The paper is organized as follows. Section II formulates the general learning problem in a domain-parameterized setting. Section III presents the proposed domain-adaptation framework using unfolding-based networks. Sections IV, V, and VI

describe its application to noise adaptation, gain calibration, and phase retrieval, respectively, followed by conclusions.

II. PROBLEM FORMULATION

Consider a learning problem from a set of paired data points $\mathcal{D} = \{\mathbf{y}_n, \mathbf{x}_n\}_{n=1}^N$ where $\mathbf{y}_n \in \mathbb{C}^{N_y}$ is input or feature to a network to be learned and $\mathbf{x}_n \in \mathbb{C}^{N_x}$ is the corresponding output or label. The terms N_y and N_x denote the dimensions of the input and output vectors, respectively. Here, N represents the sample count of the dataset. The objective is to learn a function or a network $f_{\alpha, \beta} : \mathbb{C}^{N_y} \rightarrow \mathbb{C}^{N_x}$, with the learnable parameters (α, β) , such that the estimate $f_{\alpha, \beta}(\mathbf{y}_n)$ is close to the true output \mathbf{x}_n in a predefined distance metric. The goal is typically achieved by fine-tuning the learnable parameters by solving the following optimization problem:

$$\min_{\alpha, \beta} \sum_{(\mathbf{y}_n, \mathbf{x}_n) \in \mathcal{D}} d(\mathbf{x}_n, f_{\alpha, \beta}(\mathbf{y}_n)), \quad (1)$$

where $d(\cdot, \cdot)$ is a distance metric in \mathbb{C}^{N_x} . The parameters learned through the process are optimal for the training data \mathcal{D} . It is expected that for any unseen data pairs, the learned network will provide fairly accurate results, given that the unseen or test data is similar to the training data. The similarity is generally ascertained by assuming that the train and test data are sampled from the same probability distribution.

In many practical applications, the data set could be parameterized as \mathcal{D}_θ where θ is the parameter vector whose entries could be either discrete or continuous values. For example, θ could represent the noise level in the features/input. Since the data changes with θ , an important question arises on how to train the network in this scenario. For the simplicity of the discussion, let us assume that θ can take on one of the following J values: $\{\theta_j\}_{j=1}^J$, where J denotes the number of distinct domains in the training set. Then we can have the following training options.

The first is to train individual networks for each data set \mathcal{D}_{θ_j} . Such PT approach results in the learnable parameters $\{\alpha_j, \beta_j\}$ as a result of the following optimization problem,

$$\{\alpha_j, \beta_j\} = \arg \min_{\alpha, \beta} \sum_{(\mathbf{y}_n, \mathbf{x}_n) \in \mathcal{D}_{\theta_j}} d(\mathbf{x}_n, f_{\alpha, \beta}(\mathbf{y}_n)). \quad (2)$$

The PT method requires training J networks, which may not be practically feasible, especially when θ is a continuous variable. In addition, during inference, the precise value of θ should be known such that the corresponding network is used. Any mismatch may amplify the inference error.

To reduce the number of networks to be trained, a JT strategy could be used. Here, a single network is trained for all the data as

$$\{\alpha_{\text{joint}}, \beta_{\text{joint}}\} = \arg \min_{\alpha, \beta} \sum_{j=1}^J \sum_{(\mathbf{y}_n, \mathbf{x}_n) \in \mathcal{D}_{\theta_j}} d(\mathbf{x}_n, f_{\alpha, \beta}(\mathbf{y}_n)). \quad (3)$$

Unlike PT, in the JT approach, knowledge of the precise value of θ is not required. However, this approach may have an inferior performance compared with PT due to combined training. The reduction in performance depends on how the

data parameter θ is related to the data and hence, varies for different models.

Transfer learning and domain adaptation methods offer an alternative solution to this problem. In transfer learning, a general-purpose pre-trained network, let us say, on data set \mathcal{D}_{θ_1} , is retrained for a new data set, say \mathcal{D}_{θ_2} [1], [2], [3], [4]. While retraining, most layers are fixed, and the remaining ones, usually the last few, are relearned for the new data. For example, let f_{α_1, β_1} is the network learned on \mathcal{D}_{θ_1} . Then, during fine-tuning or retraining, the parameters α_1 are kept fixed, and the parameters β are learned. The pretraining and fine-tuning steps for the example considered here are given below.

$$\text{Pre-training: } \{\alpha_1, \beta_1\} = \arg \min_{\alpha, \beta} \sum_{(\mathbf{x}_n, \mathbf{y}_n) \in \mathcal{D}_{\theta_1}} d(\mathbf{x}_n, f_{\alpha, \beta}(\mathbf{y}_n)).$$

$$\text{Fine-tuning: } \{\beta_2\} = \arg \min_{\beta} \sum_{(\mathbf{x}_n, \mathbf{y}_n) \in \mathcal{D}_{\theta_2}} d(\mathbf{x}_n, f_{\alpha_1, \beta}(\mathbf{y}_n)).$$

The fine-tuning-based method to adapt a network for new data is typically applied in classification tasks where the first few layers are assumed to act as feature extractors. The last few layers, which are retrainable, work as classifiers. The features could be the same for different data sets; hence, only the classifier must be tuned. However, in conventional DNNs/CNNs, it is not straightforward to differentiate between feature extractor layers and classification layers. The method may also not be directly applicable to regression tasks, which are of interest in this work. A principled discussion on when this small tunable subset assumption is expected to hold, along with a practical diagnostic procedure to select the tunable subset and typical failure cases, is discussed below;

A. Selecting Tunable Subset

The standard fine tuning view, which divides a network into a domain-invariant section and a tiny domain-specific section, is what we employ in the study. The network is expressed concretely as $f_{\alpha, \beta}$, where α remains constant and only β is modified for a new domain. Choosing β to capture the majority of the domain variation while minimizing the adaptation cost is the aim of this study.

B. When the assumption holds

The selection (α, β) will hold when,

- 1) The domain shift affects specific, identifiable aspects of the forward model or the underlying iterative algorithm.
- 2) The unfolded network architecture is derived from a parametric optimization algorithm where certain parameters have clear physical interpretations (e.g., the threshold parameter in soft-thresholding corresponds to noise level in ISTA/LISTA).
- 3) The domains share a common underlying signal structure, differing only in observation conditions (e.g., same signal class with varying SNR).

C. Typical failure cases

Adapting only a small subset may fail when,

- 1) *Domain shift is hard to describe*: If the changes across domains cannot be expressed through a set of meaningful variables, or if it cannot be linked to any identifiable component of the forward model or the underlying iterative algorithm, then it is unclear which internal parameter should be treated as tunable, and tuning only a small subset may not work.
- 2) *Signal type itself changes across domains*: If the signal class itself changing across domains, then there may not be a common reconstruction method that works for all domains. \mathbf{x} may have different priors in different domains. The same unfolded backbone may no longer be appropriate even when the forward model is unchanged. For example, consider a fixed imaging operator $\mathcal{A}(\cdot)$ (same blur kernel or same sensing matrix), but one domain consists of cartoon-like images with large flat regions and sharp edges, while another domain consists of real RGB photographs with rich textures and fine details. The forward model can be the same across domains,

$$\mathbf{y} = \mathcal{A}(\mathbf{x}) + \boldsymbol{\eta},$$

but the *signal class* \mathbf{x} can change from cartoon-style images (piecewise-constant with sharp edges) to real RGB photographs (rich textures). In such cases, tuning a small subset of parameters may not be sufficient, and a larger part of the model may need to be redesigned or adapted.

- 3) *Non-interpretable architectures*: For black-box DNNs without clear parameter-to-physics mappings, identifying which parameters should be tunable becomes non-trivial and requires purely data-driven variance analysis, by checking which parameter vary the most across domain-specific trainings [17].

D. Diagnostic procedure to identify β and α

For a new task, a simple and practical diagnostic can be followed that can leverage from the interpretability of the unfolded model or for no-clear interpretability, an empirical cross-domain stability check,

- 1) *Interpretable parameter selection*: use the algorithmic interpretation of the unfolded network to propose a small candidate set of tunable parameters (e.g., soft-threshold parameters in LISTA-type layers for noise variation, or calibration-related blocks for gain variation), while treating the remaining parameters as α .
- 2) *Cross-validation parameter selection*: Train J domain-specialist models (PT) on $\{\mathcal{D}_{\theta_j}\}_{j=1}^J$ and compute how much each parameter block changes across domains. Let $\phi^{(m)}$ denote the m -th parameter block of the unfolded model (e.g., a step-size block, a shrinkage/regularization block, or any other grouped set of learnable parameters).

Define the mean block

$$\bar{\phi}^{(m)} = \frac{1}{J} \sum_{j=1}^J \phi_j^{(m)}, \quad (4)$$

and a normalized cross-domain deviation score

$$\Delta_m = \frac{1}{J} \sum_{j=1}^J \frac{\|\phi_j^{(m)} - \bar{\phi}^{(m)}\|}{\|\bar{\phi}^{(m)}\| + \epsilon}, \quad \epsilon > 0. \quad (5)$$

Blocks with small Δ_m are treated as domain-invariant and assigned to α , while blocks with large Δ_m are treated as domain-sensitive and assigned to β .

To validate this split, freeze α and retrain (or fine-tune) only β using mixed-domain training data; if the resulting performance is close to PT on all domains, the split is accepted. If there is a clear performance gap, move the next-most-variable blocks (based on Δ_m ranking) from α to β and repeat.

In the previous approach, once the network is pre-trained on data \mathcal{D}_{θ_1} , the data is no longer used during fine-tuning for dataset \mathcal{D}_{θ_2} . Note that the data from \mathcal{D}_{θ_1} and \mathcal{D}_{θ_2} have different distributions, and in the fine-tuning approach, there is no emphasis on distribution alignment. On the other hand, in the supervised domain-adaptation methods, data from all the distributions are used simultaneously to train a network [18], [19], [20], [21]. However, the JT baseline in (3), does not include such alignment and trains on pooled data directly. Though these methods seem suitable for the problem considered in this paper, the approaches do not consider the parametric relationship among the data, which is prevalent in many applications. Further, most notable works in transfer learning and supervised domain adaptation focus on classification tasks, and it is unclear how to extend them to regression problems, except for a few works [22], [23], [24], [25], [26], [27]. Again, these works treat each domain independently and do not consider any underlying parametric relationship.

In regression tasks such as denoising and deblurring, plug-and-play (PnP) methods [28] adapt the regularizer by embedding a denoiser into the optimization, making the inference robust to varying data statistics. Our work is related in spirit, as both PnP and TDA introduce adaptivity into model-based inference. The key distinction is that PnP relies on implicit priors through denoisers, whereas TDA introduces explicit, interpretable tunable parameters (such as β) to handle domain shifts such as noise or gain.

III. DOMAIN-ADAPTATION THROUGH UNFOLDING

In this section, we discuss the proposed method for adapting a network from the data. In the fine-tuning approach discussed in the previous section, only β is learned for the new data. As discussed, in DNNs/CNNs, though there is intuitive reasoning about it, it has not been proven theoretically why only a certain part of the networks should be tuned. Additionally, the layers of a DNN or a CNN are not interpretable, which makes it challenging to prove the tuning part. Unlike DNNs/CNNs, unfolding (or unfolding)-based methods, which are deep learning models that are derived by unfolding an iterative optimization

algorithm into a finite number of layers, are interpretable [15], [12]. These networks incorporate domain-specific knowledge from optimization techniques and leverage the power of deep learning for efficient and interpretable learning. By noting that the parametric relationship between the domains stems from physical models that generate data and unfolding networks are domain and model-specific, we show that fine-tuning can be made interpretable and efficient.

To elaborate on the interpretable domain adaptation via unfolding framework, let $f_{\alpha,\beta}(\cdot)$ be the unfolded network. Unlike standard DNNs/CNNs, the learnable parameters $\{\alpha, \beta\}$ in this network are model-specific and interpretable. When the network is trained on parametric data \mathcal{D}_{θ} , the network's parameters $\{\alpha, \beta\}$ are function of θ . In the following, we assume that among these, α changes negligibly with θ , whereas, β strongly depends on θ . Mathematically, there exist a function $g(\cdot)$ such that

$$\beta = g_{\varphi}(\theta), \quad (6)$$

where φ are parameters of the function. The function $g(\cdot)$ can be either derived from the physics of the generating model or learned from the available data. The assumption of the existence of g_{φ} is the same as in the fine-tuning approach. However, the assumption holds in practice for many unfolding networks and parametric data, as shown in the following sections. A P-TDA approach is used for known g and θ , to learn the network as

$$\min_{\alpha} \sum_{j=1}^J \sum_{(\mathbf{y}_n, \mathbf{x}_n) \in \mathcal{D}_{\theta_j}} d(\mathbf{x}_n, f_{\alpha, g_{\varphi}(\theta_j)}(\mathbf{y}_n)). \quad (7)$$

The resulting network $f_{\alpha, g_{\varphi}(\theta)}(\cdot)$ can then be adapted to test data coming from any domain by substituting appropriate θ . When g_{φ} is unknown and θ is known, it can be learned by solving the problem

$$\min_{\alpha, \varphi} \sum_{j=1}^J \sum_{(\mathbf{y}_n, \mathbf{x}_n) \in \mathcal{D}_{\theta_j}} d(\mathbf{x}_n, f_{\alpha, g_{\varphi}(\theta_j)}(\mathbf{y}_n)). \quad (8)$$

In practice, g_{φ} is realized using a neural network where the inputs are the domain information θ_j as well as the measurements \mathbf{y}_n s. In addition, the parameters to the forward model can be used. We observe that the additional information of the measurements improves the performance of the overall tunable network.

In the case of unknown g and θ , we propose the following DD-TDA approach. By noting that the data is implicitly dependent on θ , we train a function $h_{\varphi}(\cdot)$ which is expected to estimate β from the data. Specifically, we optimize the following problem

$$\min_{\alpha, \varphi} \sum_{j=1}^J \sum_{(\mathbf{y}_n, \mathbf{x}_n) \in \mathcal{D}_{\theta_j}} d(\mathbf{x}_n, f_{\alpha, h_{\varphi}(\mathbf{y}_n)}(\mathbf{y}_n)). \quad (9)$$

The proposed method results in a single tunable network $f_{\alpha, h_{\varphi}(\cdot)}(\cdot)$. Note that during inference, for any test input \mathbf{y} , the network not only predicts the output but also tunes the network via the function h_{φ} . As in the previous model, the function h_{φ} is realized using a neural network.

In the aforementioned formulation, the network $f_{\alpha, h_{\varphi}(\cdot)}(\cdot)$ is trained over the domains $\{\theta_j, j = 1, \dots, J\}$. The network is expected to adapt well to any data from the trained domains. However, whether it will perform well on an unseen domain $\theta \notin \{\theta_j, j = 1, \dots, J\}$ depends on the generalization ability of the function $h_{\varphi}(\cdot)$. As we will show in the following sections, the generalization ability depends on the task and how the domain parameter depends on the network parameter. In general, the generalization is good for large J , as with any learned network, where the generalization typically improves with the data size.

We would like to emphasize that P-TDA is primarily intended as a *proof-of-concept benchmark* that illustrates the performance upper bound when an ideal domain parameter θ is available and used to tune β via a mapping. Additionally, we considered comparing P-TDA to cross-validation-based selection of β , but it is impractical in our setting due to (i) the lack of a well-defined candidate set, and (ii) the need for repeated tuning across domains, which hinders scalability under continuous or high-dimensional shifts. In contrast, DD-TDA learns a data-driven mapping to β without requiring access to σ or per-domain tuning, making it more suitable for adaptive scenarios with latent or dynamic domain factors.

In the following sections, we consider three practical scenarios of the aforementioned framework. In particular, we discuss domain adaptation for compressive sensing in the next section, followed by adaptation for blind calibration problems, and finally adaptive phase retrieval.

IV. NOISE-ADAPTIVE TUNABLE LISTA

This section considers the first problem of domain adaptation through tunable unrolled networks. The problem is to recover sparse vectors from their compressed measurements under different noise conditions. Before detailing the problem and the proposed solution, we first give a quick background of the compressive sensing problem, its solution, and LISTA.

A. The Compressed Sensing Problem

Consider a set of noisy linear measurements as

$$\mathbf{y} = \mathbf{A}\mathbf{x} + \boldsymbol{\eta}, \quad \boldsymbol{\eta} \sim \mathcal{N}(\mathbf{0}, \sigma^2 \mathbf{I}_{N_y}), \quad (10)$$

where $\boldsymbol{\eta} \in \mathbb{R}^{N_y}$ is an additive Gaussian noise vector with mean $\mathbf{0} \in \mathbb{R}^{N_y}$ and covariance $\sigma^2 \mathbf{I}_{N_y}$. Here, $\mathbf{y} \in \mathbb{R}^{N_y}$ representing the measurement signal, $\mathbf{x} \in \mathbb{R}^{N_x}$ denoting the unknown signal to be estimated, and $\mathbf{A} \in \mathbb{R}^{N_y \times N_x}$ signifying the measurement matrix with $N_y < N_x$. The underdetermined system of equations can be solved with a sparsity assumption on \mathbf{x} , that is, $\|\mathbf{x}\|_0 \leq L$ where $L < N_y$. A widely used approach to solve the problem is to minimize the following ℓ_1 -minimization problem:

$$\min_{\mathbf{y}} \|\mathbf{y} - \mathbf{A}\mathbf{x}\|_2^2 + \lambda \|\mathbf{x}\|_1. \quad (11)$$

The objective function encourages solutions that balance data fidelity, captured by the first term, and sparsity, controlled by $\|\mathbf{x}\|_1$. The balance can be achieved by choosing the hyperparameter λ appropriately. Several practical algorithms,

such as the basis pursuit, iterative hard-thresholding, and ISTA [14], [29], have been developed to solve the optimization problem.

Most of the aforementioned algorithms are iterative and, starting from an initial estimate, refine the estimate in each iteration. For example, let \mathbf{x}^k be the current estimate of the sparse signal at iteration k , \mathbf{x}^{k+1} is the updated estimate for the next iteration. The update rule in ISTA is given as

$$\mathbf{x}^{k+1} = \mathcal{S}_{\beta} (\mathbf{W}_1 \mathbf{y} + \mathbf{W}_2 \mathbf{x}^k), \quad (12)$$

with

$$\mathbf{W}_1 = \frac{1}{\kappa} \mathbf{A}^T, \quad \mathbf{W}_2 = \mathbf{I}_{N_x} - \frac{1}{\kappa} \mathbf{A}^T \mathbf{A}, \quad \text{and} \quad \beta = \frac{\lambda}{\kappa}, \quad (13)$$

where \mathbf{I}_{N_x} is the $N_x \times N_x$ identity matrix and \mathcal{S}_{β} is an elementwise soft-thresholding operation with threshold parameter $\beta = \frac{\lambda}{\kappa}$ where κ is greater than the largest eigenvalue of $\mathbf{A}^T \mathbf{A}$.

While ISTA and other algorithms work well in practice, their convergence is slow. In addition, the methods are data-independent. On the other hand, given a set of data with some underlying structure (for example, drawn from the same distribution), the algorithms should be able to be fine-tuned to improve the performance. Additionally, LISTA achieves lower recovery error in fewer layers compared to the ISTA with the same number of iterations. This is precisely the LISTA [15] algorithm where the matrices $\boldsymbol{\alpha} = \{\mathbf{W}_1, \mathbf{W}_2\}$ together with the thresholding parameter β are learned from the data by keeping the number of iterations fixed. The LISTA is shown to converge in fewer iterations than the original ISTA.

Before we discuss the proposed noise-adaptive LISTA, we quickly summarize a few results on adaptive LISTA approaches and compare them with the current one.

B. Variations of LISTA

In the original LISTA framework [15], the network is trained to learn the parameters $\{\mathbf{W}_1, \mathbf{W}_2, \beta\}$ (cf. (13)) using data generated from a specific distribution and a known measurement matrix \mathbf{A} . Changes in \mathbf{A} lead to changes in the distribution, affecting the measurements \mathbf{y}_n and necessitating network retraining. To address this, [30] introduced an adaptive LISTA algorithm where matrices $\mathbf{W}_{1,2}$ are decomposed into two parts: a fixed component dependent on \mathbf{A} and a learnable component similar to traditional LISTA. This enables training on data generated by multiple choices of \mathbf{A} , optimizing the network accordingly. At inference, the network adapts to new \mathbf{A} before prediction, demonstrating improved performance across varying \mathbf{A} values with theoretical guarantees. However, this method requires precise domain parameter knowledge (here \mathbf{A}) during inference, and the matrix decompositions introducing domain dependence are less straightforward, leaving room for alternative approaches [31], [32], [33]. While our focus differs, our DD-TDA framework does not necessitate prior domain parameter knowledge. In cases where it is known, we optimize its use akin to the P-TDA approach.

Another line of work reduces reliance on learning. Analytic-LISTA [32] shows that $\mathbf{W}_{1,2}$ can be analytically derived from \mathbf{A} , eliminating the need to learn them. Li *et al.* [34]

TABLE I
TEST RESULTS OF RETRAINED DNNs FOR DOMAIN ADAPTATION

Training approach	D1(6 dB)	D2(16 dB)	D3(31 dB)
NMSE (in dB), HR(%)			
Joint train	-6.60, 54.22	-12.34, 76.72	-13.33, 79.81
Retrain last layer	-6.72, 53.73	-12.64, 77.87	-13.79, 81.17
Retrain last 3 layers	-7.10, 53.93	-13.92, 83.40	-16.17, 89.24

proposed an error-based thresholding scheme, where the layer-wise threshold is set as a function of the reconstruction error. Chen *et al.* [33] further enhanced LISTA by adding momentum, yielding practical rules for adaptively calculating layer parameters and improving both generalization and training efficiency.

While these approaches introduce adaptivity at the algorithmic or parameter level, our focus is complementary: the proposed DD-TDA framework learns to adjust domain-sensitive parameters *without requiring prior knowledge of the domain*, while P-TDA leverages domain knowledge when it is available.

C. Noise-Level-Specific Domains

In this problem, noise variance parameterized the domains, and the domain-specific measurements are given as

$$\mathcal{D}_{\theta_j=\sigma_j} = \{\mathbf{y}_{ij}, \mathbf{x}_i\}_{i=1}^N \quad \forall j = \{1, 2, \dots, J\}, \quad (14)$$

where

$$\mathbf{y}_{ij} = \mathbf{A}\mathbf{x}_i + \boldsymbol{\eta}_j, \quad \boldsymbol{\eta}_j \sim \mathcal{N}(\mathbf{0}, \sigma_j^2 \mathbf{I}_{N_y}), \quad (15)$$

and \mathbf{I}_{N_y} is an identity matrix of dimension $N_y \times N_y$.

Specifically, for each domain, the noise levels are different while the rest of the measurement model remains fixed. The measurement model is practically relevant, as the noise levels can vary significantly. As discussed in Section II, both the PT and JT approaches have limitations. Here, we consider the problem of fine-tuning the LISTA model to adapt it to different noise domains.

For ease of discussion, the different domains, based on the noise levels, are also characterized by average SNR levels defined as

$$\text{SNR}_j = \frac{1}{N} \sum_{i=1}^N 10 \log_{10} \left(\frac{\frac{1}{N_y} \|\mathbf{A}\mathbf{x}_i\|_2^2}{\sigma_j^2} \right). \quad (16)$$

D. A Retraining Approach

Before introducing our noise-tunable LISTA framework, we first examine the effectiveness of a retraining-based method that utilizes a DNN to address the noise-tunability challenge. The experiment is conducted on a dataset with three domains with SNRs of 6 dB, 16 dB, and 32 dB. Data is generated following (14) and (15) (see the data generation part of Section IV-E for details). We start by training a fully connected neural network on a combined dataset containing samples from all domains. The network consists of three hidden layers with 256, 512, and 256 neurons, respectively, each followed by

ReLU activations. For domain-specific adaptation, we perform staged retraining by progressively unfreezing deeper layers of the network on the target domain data. For retraining, we use domain-specific data that was previously included in a mixed-domain dataset during the initial training phase. Initially, only the final layer is retrained; then, we freeze the first hidden layer and fine-tune the remaining layers, including the output layer. Results in Table I show that retraining just the final layer does not yield significant improvements across varying noise levels. However, as more layers are made trainable, performance on the test data, measured in terms of NMSE and HR (defined in (18) and (19)), improves consistently. These findings suggest that adapting only the final layer is insufficient for effective tunability. Instead, identifying the optimal subset of layers to retrain may require a trial-and-error approach, which can be task-specific and assumes access to domain-specific data for adaptation.

E. Proposed Noise-Adaptive LISTA (NA-LISTA)

Unlike the previous DNN-based methods, we show that LISTA is tunable to noise levels. Specifically, we note that among the learnable parameters of LISTA, $\boldsymbol{\alpha} = \{\mathbf{W}_1, \mathbf{W}_2\}$ and β , the latter one is a strong function of the noise variance σ for a fixed \mathbf{A} , that is, we have that $\beta = g(\sigma)$. There are several choices of g [35] and one of the widely used ones is given as [16]

$$\beta = \sigma \sqrt{2 \log N_x / \kappa}. \quad (17)$$

The above formulation implies that the higher the noise variance, the larger the soft thresholding is. Since the soft-thresholding operation promotes sparsity, a larger β generates sparser estimates. The choice in (17) requires precise knowledge of σ , which may not be available in practice and has to be estimated using different methods [35], [36], [37]. An alternative approach is cross-validation [38] where β is learned from validation data. The learned parameter is not optimal if the validation data consists of measurements with various noise levels.

To address the limitations mentioned above, we apply the proposed P-TDA (assuming a known σ) and DD-TDA methods. One iteration or layer of these two methods, including the conventional LISTA, are shown in Fig. 1. In P-TDA, $\{\mathbf{y}, \sigma\}$ are used to tune the network by altering β , whereas, in DD-TDA framework, only $\{\mathbf{y}\}$ is given as input to h_φ to tune β . In the following, we discuss the data generation and results.

Data Generation and Network Architecture: To evaluate the proposed NA-LISTA, we generated a synthetic dataset as per (14)–(15). The matrix \mathbf{A} was kept fixed in all the experiments, and its entries were sampled from a standard normal distribution followed by columnwise normalization. Further, we set $N_x = 100$, $N_y = 30$, and $L = 3$. The entries of the noise vector were zero-mean Gaussian random variables with domain-specific standard deviations. Specifically, noise variance σ_j simulates J distinct SNR levels for robustness assessment. The total number of samples generated was split into train, validation, and test sets in the ratio of 56%, 24%, and 20%, respectively.

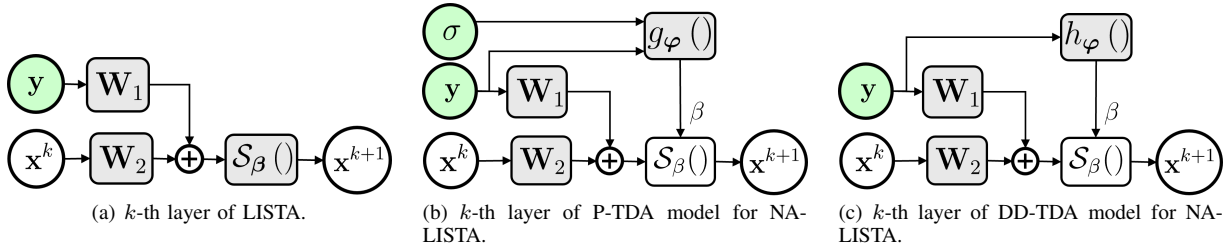


Fig. 1. Layers/iterations of different LISTA architectures: (a) Conventional LISTA, (b), (c) NA-LISTA. (b) Single layer of the P-DTDA model with input data $\{y, \mathbf{A}\}$ and domain parameter σ available during inference. (c) Single layer of DD-TDA model with only input data $\{y, \mathbf{A}\}$ available during inference. Note: Green blocks represent the data available at inference time, and Gray blocks are trainable parameters.

Since samples from all the domains were used to train and test the JT, P-TDA, and DD-TDA methods in order to maintain dataset size uniformity, we used the same number of samples for each PT model. For example, for the J domains used for training, we generated N_{train} (training set slice of N) examples from each domain, and used $N_{train} \times J$ training samples for JT, P-TDA, and DD-TDA methods. Whereas, we generated $N_{train} \times J$ examples for training each domain-specific PT model. In the following experiments, we consider $J = 3$ and $N = 43,000$.

LISTA networks with the proposed g_φ and h_φ networks were jointly trained in an end-to-end fashion using backpropagation, and the mean-squared error (MSE) loss was used as the cost function. The MSE was measured by averaging the Euclidean distance $\|\mathbf{x}^* - \hat{\mathbf{x}}\|_2^2$ over the training batch, where \mathbf{x}^* and $\hat{\mathbf{x}}$ denote the ground truth and predicted sparse signals, respectively. The network parameters were initialized as mentioned in (13), where λ was initialized to 0.1 and κ was 1.001 times the maximum absolute eigenvalue of $\mathbf{A}^T \mathbf{A}$. Further, in our experiments, all methods, PT, JT, P-TDA, and DD-TDA, assume that the sensing matrix \mathbf{A} is known and fixed, ensuring a fair comparison. In all the methods, \mathbf{W}_1 and \mathbf{W}_2 are initialized using \mathbf{A} .

Performance Metrics: Model performance was evaluated using Normalized Mean Squared Error (NMSE) and Hit Rate (HR). Let \mathbf{x}^* be the ground truth signal and $\hat{\mathbf{x}}$ be the predicted sparse signal. The NMSE contribution by each test sample is given by

$$\text{NMSE} = \frac{\|\mathbf{x}^* - \hat{\mathbf{x}}\|_2^2}{\|\mathbf{x}^*\|_2^2}. \quad (18)$$

For our experiments, the average NMSE over the entire test set was computed and reported in decibels.

The HR, with a relative error tolerance t , is defined as

$$\text{HR} = \frac{\sum_{n=1}^{N_x} \mathbb{1}(\mathbf{x}^*(n) \neq 0) \mathbb{1}(|\mathbf{x}^*(n) - \hat{\mathbf{x}}(n)| \leq t \mathbf{x}^*(n))}{L}. \quad (19)$$

Here, n indexes the elements of the vectors \mathbf{x}^* and $\hat{\mathbf{x}}$. HR measures the fraction of nonzero entries in $\hat{\mathbf{x}}$ whose estimates fall within a relative error tolerance of t , set to 0.3 in our experiments. For our experiments, the average HR (in %) over the entire test set is reported.

Experiments: We conducted three evaluations. The first one focused on a broad range of SNRs, another covers a lower

SNR range, and a third for testing generalization by evaluating on unseen SNR levels. The first two experiments were designed to test whether the proposed method can generalize across domains with large variations in noise level, as well as when domain shifts are subtle and more challenging to distinguish. In each of these, our proposed DD-TDA and P-TDA methods were compared with the baseline JT and PT methods. For both JT and PT, conventional LISTA networks were trained.

Comparison with the existing methods: For the broad range we considered three noise levels as D1 ($\sigma = 0.1$, SNR = 6 dB), D2 ($\sigma = 0.03$, SNR = 16 dB), and D3 ($\sigma = 0.005$, SNR = 32 dB). For the narrow range, the SNRs are given as D1 ($\sigma = 0.12$, SNR = 4 dB), D2 ($\sigma = 0.06$, SNR = 10 dB), and D3 ($\sigma = 0.035$, SNR = 15 dB). For these two scenarios, the NMSEs and HRs of the methods when tested for each domain are shown in Figs. 2(a) and IV-E. Here, PT-D1, PT-D2, and PT-D3, refers to PT methods trained for domains D1, D2, and D3, respectively. We observe that PT methods trained for a specific domain generally perform well when tested on the same domain. Specifically, the observation is true in terms of NMSE, but not always in terms of HR, as it is a stricter metric and can exhibit more variability. The performance deteriorates when trained and tested on different domains. Further, PT gives lower error (better HR) than JT for all the domains, and this observation is more evident in the HRs, where PT shows a performance improvement of 11 – 16% over the JT for D2 and D3. We note that the JT and PT perform similarly on D1, likely because PT-D1 was trained only on highly noisy samples, unlike JT, which saw both clean and noisy data, leading to PT-D1 underperforming relative to expectations.

Comparing the proposed P-TDA and DD-TDA with the PT method, we observe that the proposed approaches are performing on par with the respective PT methods for each domain. Focusing on the DD-TDA method, which does not consider the domain knowledge, and has comparable performance with the PT methods. The only notable performance gain of PT over our methods is that in D3 during the broad SNR range experiment, with an NMSE gain of around 5 dB, likely due to PT-D3 having access to significantly more clean training examples than the DD-TDA method. In Fig. 2, we now provide an example reconstruction from the D2-domain for visual comparison. The plots clearly illustrate the estimation

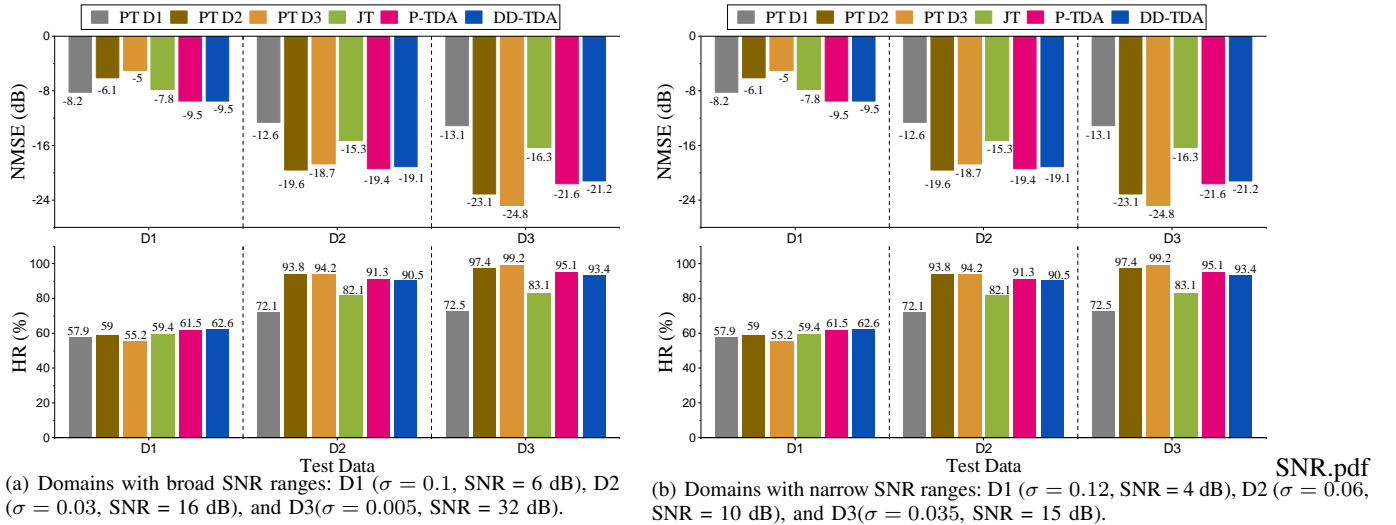


Fig. 2. Comparison of the proposed methods with the JT and PT methods for NA-LISTA for different SNR ranges. PT’s performances are better than JT’s for each domain. The P-TDA/DD-TDA has comparable performance to PT, demonstrating the noise-tunability aspect.

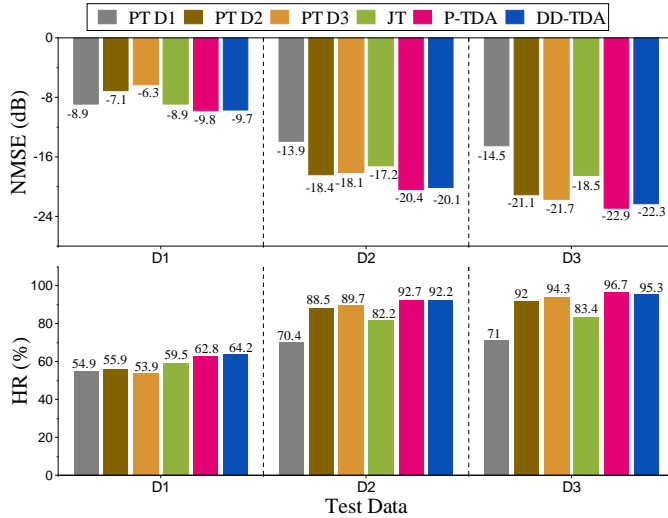


Fig. 3. Comparison of the proposed methods with the JT and PT methods for NA-LISTA for broad SNR ranges, averaged over 5 experiments.

accuracy and highlight the improvements achieved by the proposed methods, complementing the quantitative results. In a nutshell, the results show the tunability aspect of the NA-LISTA for different noise levels. In Fig. 3, we show the metrics averaged over five repetitions of the experiments from a broad-SNR range. For NA-LISTA, DD-TDA occasionally matches or even outperforms P-TDA due to: (i) its end-to-end task-specific learning of β , (ii) the limited flexibility of P-TDA’s fixed mapping from σ to β , (iii) implicit regularization effects in DD-TDA that enhance robustness, and (iv) minor stochastic variations during training. To understand these variations better, in Fig. 3, we show the metrics averaged over five repetitions of the experiments from a broad-SNR range. We note that, with the repeated experiments, the observations are consistent with the previous experiments. Having assessed the fact that few network parameters are tunable with the

domains, next, we show that the remaining parameters are nearly invariant to the domains. We observe that the results of the repeated experiments agree with those of the earlier experiments. Additionally, we provide a systematic assessment of how the network parameters $\alpha = \{\mathbf{W}_1, \mathbf{W}_2\}$ and the threshold β vary with noise level $\theta = \sigma$.

F. Practical application on MNIST compressed sensing

We evaluate the proposed NA-LISTA models P-TDA and DD-TDA version, on MNIST compressed sensing reconstruction under different noise levels and compare them with recent strong baselines.

1) *Dataset Construction and Noise Model:* The MNIST dataset contains handwritten digit images of size 28×28 . Each image is vectorized as $\mathbf{x} \in \mathbb{R}^{784}$. The compressed measurements were generated using a random synthetic Gaussian sensing matrix $\mathbf{A} \in \mathbb{R}^{500 \times 784}$ with entries drawn i.i.d. from $\mathcal{N}(0, 1)$. So the compression ratio is $m/n = 500/784 = 0.638$. The training set contains 50,000 samples, and the test set contains 10,000 samples (2,000 samples per SNR level).

To model diverse real world noise like varying noise over time, or change in accusation process, the training set is divided into $J = 5$ disjoint subsets and additive white Gaussian noise at fixed SNRs of $-10, -5, 0, 5,$ and 10 dB is added per SNR subset. For a clean measurement $\mathbf{y}_{\text{clean}} = \mathbf{A}\mathbf{x}$, the noisy measurement is generated as in (15). We set the noise standard deviation σ per sample to match the target SNR as,

$$\sigma = \frac{\|\mathbf{y}_{\text{clean}}\|_2}{\sqrt{m \cdot 10^{\text{SNR}_{\text{dB}}/10}}}. \quad (20)$$

After noise addition, all subsets were concatenated and randomly shuffled to create the final training set, so the model sees mixed SNRs during training. We constructed the test set in the same way, but per SNR subsets were separated for domain-wise evaluation.

2) *Model Configurations*: We compare our methods with two strong baselines that can handle noise and use a strong image prior. Tail-LISTA, recently proposed by Kovich et al. [39], extends the learned ISTA idea by adding iterative support estimation. It alternates between signal estimation using an internal LISTA network and a tail update step that refines a support mask. This design targets robust recovery under noise and varying sparsity. Next, we use the denoising diffusion implicit model (DDIM) [40] as a baseline. DDIM is a diffusion generative model that starts from a noise sample and applies a sequence of learned denoising steps using a U-Net, which provides a strong image prior and often yields high quality image reconstructions. In our CS setup, DDIM is conditioned on the noisy measurements rather than class labels, resulting in a inference without access to labels. Exactly, the UNet receives a noise sample, a measurement conditioned input and outputs a denoised estimate at each diffusion step. This lets DDIM use a learned generative prior to produce digit-like reconstructions from compressed noisy observations, without using the true digit class.

Implementation details for fair comparison: For comparison with our $K = 15$ layer NA-LISTA models, we implemented a tight Tail-LISTA with 8 internal LISTA layers per tail step and 12 tail steps as per the paper [39]. After every tail step, we updated the support mask by choosing the top- k items by magnitude using tied weights and support-aware soft-thresholding.

Additionally, DDIM is regarded as a robust generative baseline. We employed a U-Net with base channels 128 and channel multipliers (1, 2, 4) for DDIM, and employed 50 DDIM inference steps with deterministic sampling for inference. The U-Net requires an image shaped matrix input for measurement conditioning. However, our measurement vector is $\mathbf{y} \in \mathbb{R}^{500}$ and cannot be transformed to 28×28 . To get an MNIST image shaped conditioning input, we extended the measurements by adding 284 random sub-sampled measurements form $\mathbf{y} \in \mathbb{R}^{500}$. The extended measurement vector $\hat{\mathbf{y}} \in \mathbb{R}^{784}$ is reshape to 28×28 to serve as the conditioning input to the U-Net. Finally, we normalize the images to the range $[-1, 1]$, which is a popular preprocessing method in diffusion model implementations [40].

Both P-TDA and DD-TDA use $K = 15$ tied LISTA layers. We used simple light wight MLPs as threshold prediction network, with a fully connected architecture. For DD-TDA, the MLP input is $\mathbf{y} \in \mathbb{R}^{500}$ and the layer sizes are $500 \rightarrow 750 \rightarrow 375 \rightarrow 125 \rightarrow 64 \rightarrow K$. For P-TDA, the noise level σ is also provided as domain parameter as an extra input, so the layer sizes are $501 \rightarrow 751 \rightarrow 375 \rightarrow 125 \rightarrow 64 \rightarrow K$. P-TDA takes (\mathbf{y}, σ) as input, while DD-TDA is data-driven and uses only \mathbf{y} . For JT baseline, a standard 15-layer tied LISTA trained on the same mixed-SNR data is used.

3) *Training Procedure*: All models were trained for 150 epochs using Adam optimizer with batch size 100. For P-TDA, DD-TDA, and JT, we minimized the MSE between reconstructed and ground truth images. For Tail-LISTA, we followed the original papers' idea and use a cumulative loss

TABLE II
MODEL COMPLEXITY AND INFERENCE EFFICIENCY FOR MNIST COMPRESSED SENSING. FLOPS ARE REPORTED PER SINGLE INFERENCE. P-TDA AND DD-TDA ARE NA-LISTA VARIANTS.

Model	Parameters	FLOPs	Inference Time ($\times 10^{-3}$ s)
LISTA	1,007,440	15.098 M	0.016
P-TDA	1,721,697	15.811 M	0.020
DD-TDA	1,720,0703	15.810 M	0.019
Tail-LISTA	12,089,280	96.624 M	0.117
DDIM	74,665,729	8.100 G	14.260

over all tail steps,

$$\mathcal{L}_{\text{Tail}} = \frac{1}{NM} \sum_{j=1}^N \sum_{k=1}^M \|\mathbf{x}^j - \hat{\mathbf{x}}_k^j\|_2^2, \quad (21)$$

where $\hat{\mathbf{x}}_k^j$ is the estimate after the k -th tail step for sample j with $M = 8$. DDIM is trained using the standard diffusion noise-prediction objective, predicting the injected Gaussian noise, while conditioning on the compressed measurements so that the model can reconstruct from noisy observations.

We created a validation split by taking 10% of the training set for early stopping and hyperparameter tuning. All models are trained on NVIDIA GPUs with PyTorch using a fixed random seed.

4) *Evaluation Metrics*: The reconstruction efficiency is measured using NMSE, PSNR, and SSIM. For the reconstruction quality, a downstream character recognition task is performed with optical character recognizer (OCR) accuracy as evaluation metric. Here OCR is used as a digit recognition classifier that takes the reconstructed MNIST image as input and predicts its digit label. In the MNIST setup, it is a 10 class classifier with labels from 0 to 9. Using a pretrained OCR [41], both raw accuracy and calibrated accuracy, scaled by the OCR ceiling accuracy of 97.50% on clean images, were reported.

The model's time complexity and efficiency is evaluated with total parameters, FLOPs, and inference time per sample (in mili second) measured on GPU. For JT and NA-LISTA models (P-TDA and DD-TDA), each layer computes two matrix vector multiplications $\mathbf{W}_1\mathbf{y}$ and $\mathbf{W}_2\mathbf{z}_k$ followed by soft thresholding. So the FLOPs per layer are approximately $(mn+n^2)+\mathcal{O}(n)$. With $m = 500$, $n = 784$, and $K = 15$, this gives about $\approx 15.1 - 15.9$ MFLOPs, which matches Table II. P-TDA and DD-TDA have slightly higher FLOPs due to the threshold estimator MLP overhead, but the increase is small.

Tail-LISTA uses an effective depth of 96 LISTA-equivalent iterations with tight configuration, so its FLOPs scale to about ≈ 96.6 MFLOPs. DDIM's FLOPs are dominated by running the UNet for 50 diffusion time steps, giving 8.1 GFLOPs per sample. Per sample inference time is measured by averaging many forward passes on a single GPU, excluding data loading and any post processing.

5) *Discussion*: Table II shows that the LISTA and NA-LISTA models (P-TDA and DD-TDA) are very efficient. They use about 1.0M to 1.72M parameters, about 15.1 to 15.9 MFLOPs per sample, and less than 0.020 ms inference time per sample on GPU. DDIM has the highest cost because it runs a UNet for 50 diffusion steps with 8.100 GFLOPs per

TABLE III

PER-SNR RECONSTRUCTION METRICS AND OCR ACCURACY ON MNIST TEST SET (2,000 SAMPLES PER SNR LEVEL). OCR ACCURACY CEILING ON CLEAN IMAGES IS 97.50%. P-TDA AND DD-TDA ARE NA-LISTA VARIANTS. \uparrow INDICATES HIGHER IS BETTER AND \downarrow INDICATES LOWER IS BETTER.

SNR (dB)	Model	NMSE (dB) \downarrow	PSNR (dB) \uparrow	SSIM \uparrow	Cal. Acc. (%) \uparrow	Raw Acc. (%) \uparrow
-10	LISTA [15] (JT)	-10.98	11.38	0.4036	35.07	34.55
	P-TDA (Ours)	-12.83	13.21	0.5139	51.92	51.00
	DD-TDA (Ours)	-12.19	12.61	0.5159	49.51	48.65
	Tail-LISTA [39]	-11.34	11.85	0.2857	24.07	23.55
	DDIM [40]	-11.19	11.81	0.3121	28.32	27.70
-5	LISTA [15] (JT)	-13.11	13.64	0.5773	63.99	62.90
	P-TDA (Ours)	-15.36	15.76	0.7193	83.73	82.20
	DD-TDA (Ours)	-15.39	15.80	0.7216	85.22	83.65
	Tail-LISTA [39]	-15.26	15.71	0.6286	59.28	58.20
	DDIM [40]	-15.22	15.86	0.7080	73.91	72.35
0	LISTA [15] (JT)	-16.03	16.60	0.7339	87.62	86.25
	P-TDA (Ours)	-18.30	18.85	0.8572	95.99	94.05
	DD-TDA (Ours)	-18.17	18.65	0.8414	95.17	93.10
	Tail-LISTA [39] [40]	-18.04	18.48	0.8145	85.57	83.65
	DDIM [39] [40]	-18.13	18.60	0.8339	95.62	93.25
+5	LISTA [15] (JT)	-18.47	18.99	0.8213	96.42	95.05
	P-TDA (Ours)	-21.09	21.51	0.9250	98.41	96.85
	DD-TDA (Ours)	-20.97	21.45	0.9206	98.16	96.60
	Tail-LISTA [39] [40]	-19.67	20.09	0.8842	94.32	92.70
	DDIM [39] [40]	-20.97	21.54	0.9263	98.62	97.15
+10	LISTA [15] (JT)	-19.85	20.36	0.8563	98.62	97.00
	P-TDA (Ours)	-22.49	22.84	0.9471	98.82	96.80
	DD-TDA (Ours)	-22.66	23.06	0.9489	98.82	96.80
	Tail-LISTA [39] [40]	-20.31	20.72	0.9042	96.67	94.50
	DDIM [39] [40]	-21.97	22.53	0.9417	98.62	96.80

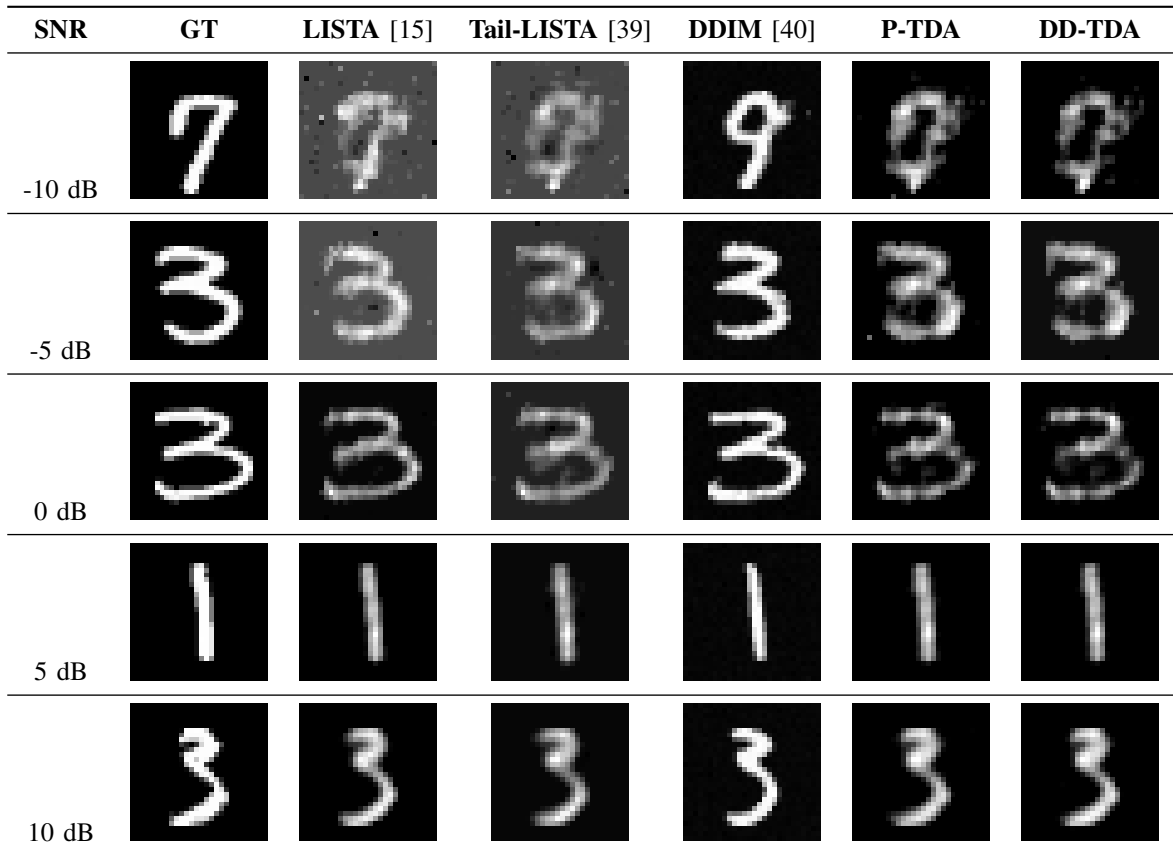


Fig. 4. Qualitative MNIST-CS reconstructions across SNR domains. Columns show ground truth (GT) and reconstructions from JT (LISTA), Tail-LISTA (tight), DDIM (diffusion model) and the proposed NA-LISTA with P-TDA and DD-TDA.

sample. Compared to DDIM with 14.260 ms, this is about a $709.5\times$ speedup, and compared to Tail-LISTA with 0.117 ms, it is about a $6.15\times$ speedup.

From Table III, at the hardest noise setting with SNR -10 dB, P-TDA is best across NMSE, PSNR, and OCR accuracy, and it also improves SSIM over LISTA and Tail-LISTA. DD-

TDA remains close to P-TDA in reconstruction quality, with slightly higher SSIM, but has lower OCR accuracy, while DDIM degrades substantially in both pixel metrics and OCR in this regime. This behavior is consistent with the qualitative results in Fig 4, when the compressed measurements are extremely noisy and contain limited class discriminative information, a strong generative prior can still produce clean, digit-like samples, but these samples may correspond to a different digit than the ground truth, which directly reduces the OCR accuracy. At SNR -10 dB, Fig. 5 shows five random MNIST-CS test examples where the compressed measurements are strongly corrupted by noise. LISTA and Tail-LISTA reconstructions contain visible background noise and broken strokes, and the digit structure is often weak in these hard cases. In contrast, P-TDA and DD-TDA produce cleaner backgrounds and better stroke continuity, which makes the digits easier to recognize visually. P-TDA results are usually slightly cleaner than DD-TDA in these examples. DDIM often generates a smooth and well-formed digit structure even under severe noise, but in some cases the generated digit shape differs from the ground truth, which suggests a possible class mismatch. This is consistent with the measurement conditioned diffusion setting, where the model can rely on its learned image prior when the measurements carry limited class information.

At low and moderate SNRs of -5 dB and 0 dB, P-TDA and DD-TDA consistently yield strong reconstruction quality and high OCR accuracy, substantially improving over LISTA (JT) and Tail-LISTA. Notably, at -5 dB, DD-TDA slightly exceeds P-TDA in SSIM and OCR accuracy even without explicit noise input, supporting the idea that the threshold network can infer noise characteristics directly from \mathbf{y} . At 0 dB, P-TDA achieves the strongest overall trade-off, delivering the best NMSE, PSNR, and SSIM along with the highest OCR accuracy, while Tail-LISTA lags in OCR accuracy despite competitive pixel-level metrics in some settings, suggesting that its support update may not preserve class-relevant structure as reliably under measurement noise.

At higher SNRs with $+5$ and $+10$ dB, all methods approach ceiling level OCR accuracy. DDIM is competitive at $+5$ dB and produces visually clean reconstructions, but at $+10$ dB the NA-LISTA variants match or slightly exceed DDIM in OCR accuracy, with DD-TDA achieving the strongest pixel level reconstruction metrics PSNR and SSIM among all methods. Across SNRs, DD-TDA typically stays close to P-TDA, indicating that explicit access to σ is most beneficial under the hardest noise, whereas in easier regimes the data-driven thresholds are sufficient. Notably, as Table II demonstrates, P-TDA and DD-TDA attain this competitive performance with roughly $7\times$ less parameters than Tail-LISTA and $43\times$ fewer than DDIM, while requiring significantly lower computational cost. In higher SNR domains, our lightweight NA-LISTA models match or surpass the more complex Tail-LISTA and DDIM baselines in both reconstruction quality and OCR accuracy, displaying that domain-aware threshold adaptation enables efficient yet accurate recovery without the overhead of deep generative priors or iterative support estimation.

Overall, P-TDA provides the best trade-off among the

TABLE IV
 $S(\mathbf{W})$ AND β VALUES FOR PT MODELS

Domains (SNR)	D1 (6 dB)	D2 (16 dB)	D3 (32 dB)
$S(\mathbf{W}_1)$	16.35	16.1	15.55
$S(\mathbf{W}_2)$	15.07	17.77	15.62
β	0.088	0.048	0.037

unfolded networks, improving both reconstruction quality and OCR accuracy over LISTA (JT) and Tail-LISTA with only a small increase in model size and runtime. DD-TDA is a strong practical option when noise levels are unknown and remains highly competitive with P-TDA across SNRs. DDIM often produces clean looking reconstructions at moderate to high SNRs, but at very low SNR it can generate a plausible looking digit that is not the true one, reducing OCR accuracy; it also requires much more computation than P-TDA and DD-TDA.

G. Invariance of α with θ

Here, we assess the variation of the network parameters $\alpha = \{\mathbf{W}_1, \mathbf{W}_2\}$ and threshold β with the noise levels $\theta = \sigma$. For NA-LISTA, it was assumed that α does not vary significantly with σ , and β changes significantly with domains. To further demonstrate invariance of $\mathbf{W}_{1,2}$ with domain shifts, in Fig. 6 showed \mathbf{W}_1 for different domains, and Figs. 7 and 8, shows zoomed-in versions of the matrices of better visualization. The images show that the values of the matrices do not vary significantly with the domains.

To assess the invariance of α across domains, we define the normalized Frobenius norm metric. To compare the structure of learned weight matrices across trained models, we define a scale-invariant metric such that it normalizes the Frobenius norm by the maximum absolute value in the matrix. Mathematically, we measured the metric $S(\mathbf{W}) = \frac{\|\mathbf{W}\|_F}{\max|\mathbf{W}|}$ and the values are shown in Table IV. The division by the maximum entry was used only as a simple normalization (in the same spirit as NMSE), so that the values are on a comparable scale. We note negligible changes in the metric for both matrices when the networks are trained for different domains. On the other hand, the values of β have a significant change with domains, justifying the assumption.

Next, we discuss the generalization ability of the proposed approaches.

H. Generalization:

Building on the previous experiments, which evaluated the model’s performance on domains with known SNR levels, we now assess its ability to generalize to unseen domains. Unlike before, the model is tested on SNR levels that were not part of the training set, allowing us to evaluate its adaptability and robustness in entirely new noise conditions. We considered six domains, D1-D6, with average SNRs (in dB) of $\{4, 10, 15, 20, 26, 32\}$. The domain-specific PT models were trained on D2, D4, and D6 datasets with N samples each. All the mix domain models, JT, DD-TDA, and P-TDA, were trained on a mix dataset of the same N samples from domains D1, D3, and D5, while they were tested on D2, D4, and D6.

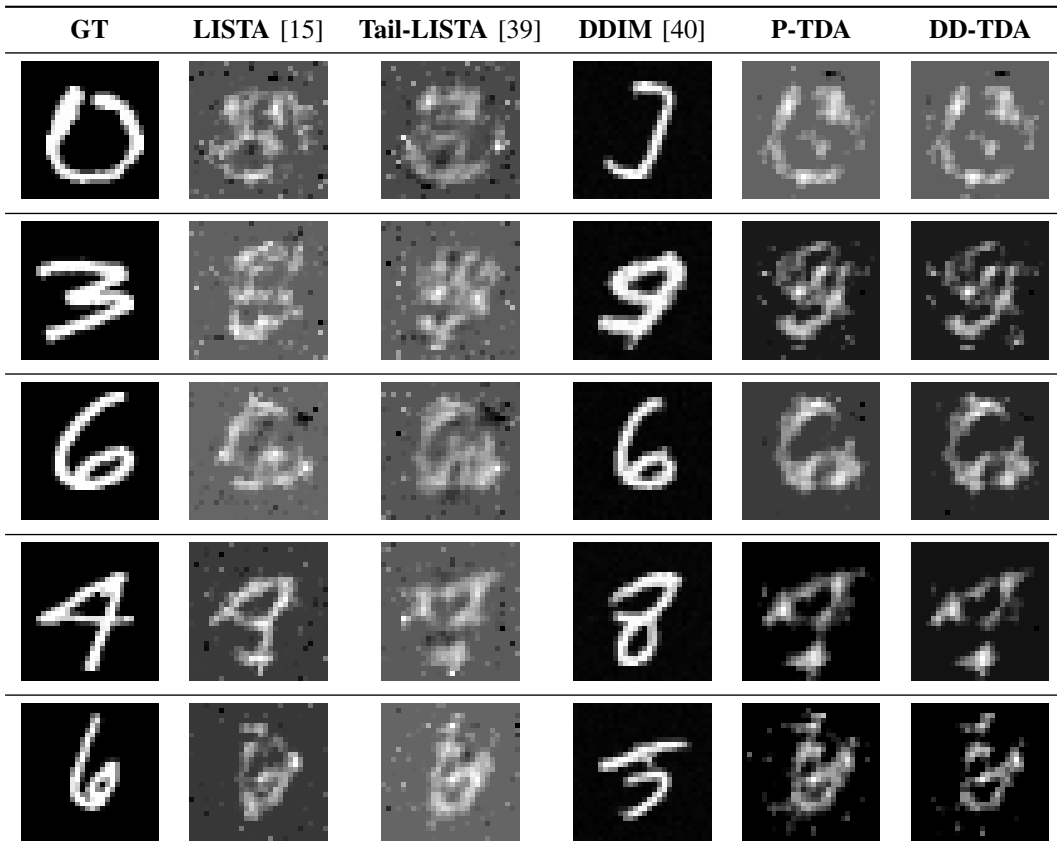


Fig. 5. Qualitative MNIST-CS reconstructions at SNR -10 dB. Columns show ground truth (GT) and reconstructions from JT (LISTA), Tail-LISTA (tight), DDIM (diffusion model) and the proposed NA-LISTA with P-TDA and DD-TDA.

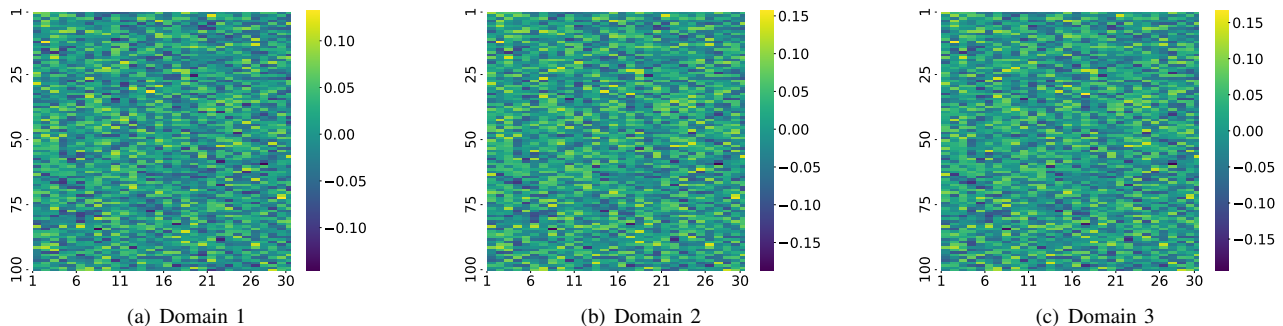


Fig. 6. Comparison of learned \mathbf{W}_1 matrices for different domains.

Since this experiment evaluates the ability to generalize to unseen domains, we compare our proposed models specifically against the JT method, focusing on their respective generalization capabilities. The results, presented in Fig. 9, demonstrate that our methods outperform the baseline JT approach, especially in the HR metric by around 9-16%. On comparing the P-TDA and DD-TDA methods with PT methods, we observe that PT methods result in a lower error of 3 – 5 dB for D4 and D6, which are high SNR domains. Whereas, for D2, with SNR of 10 dB, the P-TDA and DD-TDA have comparable performance to the PT approach. In the following, we consider another application for the P-TDA and DD-TDA methods.

V. DOMAIN-ADAPTIVE SPARSE GAIN CALIBRATION

Consider the measurements of the form

$$\mathbf{y} = \text{diag}(\mathbf{c})\mathbf{A}\mathbf{x} + \boldsymbol{\eta}, \quad (22)$$

where, except $\mathbf{c} \in \mathbb{R}^{N_y}$, the rest of the parameters have the same dimensions and characteristics as in (10). Here c_i is the gain of y_i -th measurement. In particular, \mathbf{x} is L -sparse. The measurement model is prevalent in several applications, such as time-of-flight imaging [42], [43], direction of arrival estimation with unequal sensor gains [44], and more. An unknown \mathbf{c} amounts to a sparse-blind calibration problem [45]. In [46], a data-driven approach, based on LISTA, was proposed

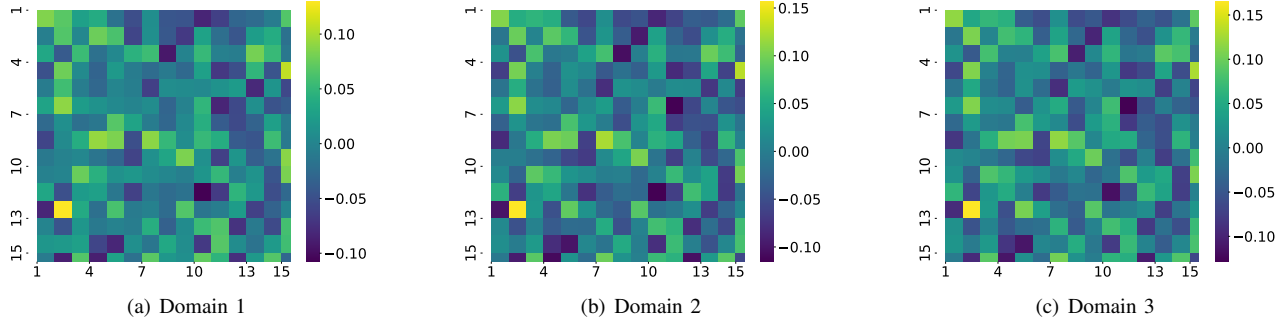


Fig. 7. Comparison of top (15×15) of learned \mathbf{W}_1 matrices.

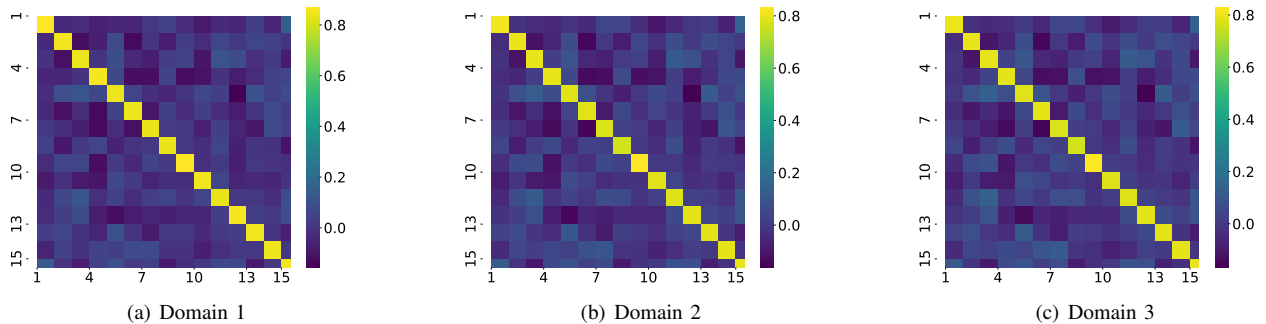


Fig. 8. Comparison of top (15×15) of learned \mathbf{W}_2 matrices for different domains.

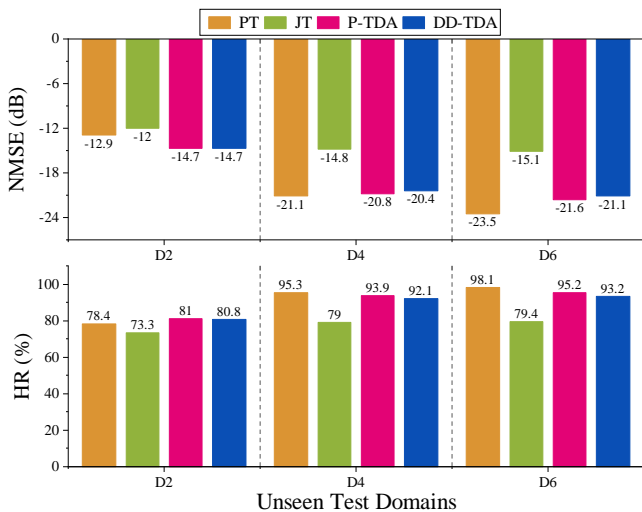


Fig. 9. Results for generalization experiment: The models (except PT) were trained on D1, D3, and D5 domains. Observation: DD-TDA generalizes well and performs better than JT models.

to solve for an unknown but fixed \mathbf{c} . However, the network has to vary as \mathbf{c} varies, which is the practice case. Here, we consider the applicability of the proposed tunability approach by considering the domain parameter as \mathbf{c} . Specifically, the data for the parametric domains are defined as

$$\mathcal{D}_{\theta=\mathbf{c}_j} = \{\mathbf{y}_{ij}, \mathbf{x}_i\}_{i=1}^N \quad \forall j = \{1, 2, \dots, J\}, \quad (23)$$

where

$$\mathbf{y}_{ij} = \text{diag}(\mathbf{c}_j)\mathbf{A}\mathbf{x}_i + \boldsymbol{\eta}_j, \quad \boldsymbol{\eta}_j \sim \mathcal{N}(\mathbf{0}, \sigma^2\mathbf{I}_{N_y}). \quad (24)$$

Note that the noise variance is constant across domains, unlike the parametric-domain model in (14) and (15). However, this is not a limitation; noise ($\boldsymbol{\eta}$) and gain (\mathbf{c}) could be the domain parameters. Since our objective is to show the tunability aspect of the network as \mathbf{c} varies, σ is kept fixed. Next, we discuss the details of the data generation and network architecture, followed by the simulation results.

A. The Proposed Approaches and Network Architecture

We first propose an approach that is applicable to both the PT and JT methods. Then, we suggest a modification to make the method domain-adaptive.

There are several possible approaches to solving the sparse-gain calibration problem. For example, one could treat $\text{diag}(\mathbf{c})\mathbf{A}$ as the measurement matrix and then apply the conventional LISTA algorithm. Alternatively, one could learn the matrices $\text{diag}(\mathbf{c})$ and \mathbf{A} separately, as in [46]. The former approach lacks adaptability, as the matrix $\text{diag}(\mathbf{c})$ is not learned independently. In contrast, the latter approach leads to a more complex network, since the information in $\text{diag}(\mathbf{c})$ is embedded within each layer of LISTA.

Another alternative, when \mathbf{c} is known, is to solve the optimization problem in (10) using LISTA, after normalizing the measurements via $\hat{\mathbf{y}} = \text{diag}(\mathbf{c}^{-1})\mathbf{y}$. However, this may

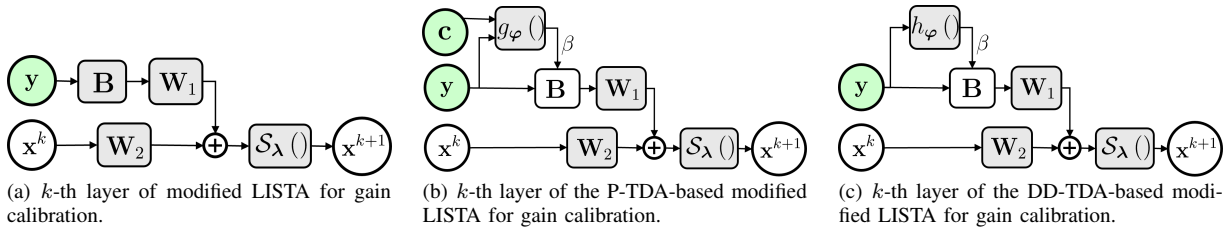


Fig. 10. Tunable model for blind calibration gain with \mathbf{B} as a tuned parameter.

significantly amplify noise in measurements corresponding to small values of \mathbf{c} — a well-known issue in deconvolution problems. Moreover, the exact values of \mathbf{c} may not be known in practice.

We address these issues by proposing an approach based on Wiener filtering for deconvolution, combined with a learning strategy. Specifically, instead of using the normalized measurements $\text{diag}(\mathbf{c}^{-1})\mathbf{y}$, we learn a vector \mathbf{b} jointly with the LISTA parameters, such that $\text{diag}(\mathbf{b})\mathbf{y}$ is used as the input to LISTA. As in Wiener filtering, the entries of the learned \mathbf{b} are expected to be small when the SNR for the corresponding measurement is low. This approach mitigates the problems associated with directly using \mathbf{c}^{-1} . Furthermore, deconvolution is performed only once, after which the subsequent layers follow the conventional LISTA structure (cf. Fig. 10(a)). The network can be trained either jointly across all domains or individually per domain to learn the parameters \mathbf{b} , $\mathbf{W}_{1,2}$ and the soft-thresholding parameter λ .

Since the domains are parameterized by the calibration vector \mathbf{c} , enabling adaptability or tunability requires identifying the parameters that vary significantly with \mathbf{c} . In Fig. 10(a), the matrix \mathbf{B} is introduced to compensate for the gain factor, while the rest of the network retains the structure of the traditional LISTA. Moreover, in the noise-free case, if one were to solve the problem using conventional ISTA, \mathbf{B} would act as \mathbf{c}^{-1} . Hence, the calibration gains $\beta = \mathbf{B}$ are expected to vary significantly with \mathbf{c} , in contrast to the parameters $\alpha = \mathbf{W}_{1,2}, \lambda$, which are relatively invariant.

Motivated by this insight, we propose the P-TDA and DD-TDA methods, as shown in Figs. 10(b) and (c), respectively. In the P-TDA method, \mathbf{B} is learned from both the known \mathbf{c} and the measurements using the network $g_\varphi(\cdot)$. In contrast, in the DD-TDA approach, \mathbf{B} is inferred solely from the measurements using the network $h_\varphi(\cdot)$.

Data Generation: For the experiment, we considered two sets of parametric domain datasets following the model in (23). The first set uses structured gains, where \mathbf{c} follows a sinusoidal distribution. Specifically, the entries of \mathbf{c} for each domain were generated as

$$\mathbf{c}_j(n) = |a \sin(2\pi f_j n + \phi_j) + b|. \quad (25)$$

The variation in \mathbf{c}_j across domains is governed by changes in $\{f_j, \phi_j\}$ and can therefore be controlled. In contrast, when $\mathbf{c}_j(n)$ was randomly generated, the resulting measurements vary significantly across domains.

In the experiments, we fixed $a = 0.5$ and $b = 0.6$, and sampled f_j, ϕ_j uniformly at random from the interval

$(0, 1]$. For the random gain scenario, each $c_j(n)$ was sampled independently from a uniform distribution over $[0.1, 1.3]$. In both the structured and random gain cases, we considered three domains ($J = 3$) and generated $N = 43,000$ examples per domain, following the procedure in Section IV-E.

The training procedures for JT, PT, P-TDA, and DD-TDA were identical to those described in Section IV.

Experiments: Using the setup, we evaluated the methods in terms of NMSE and HR. The results are shown in Figs. 11(a) and 11(b). The following observations can be made. For both gain models, the JT approach results in NMSEs that are 5–10 dB higher than those achieved by the corresponding PT approach. In the PT method, training and testing on different domains yields substantially higher errors (more than 20 dB NMSE) compared to NA-LISTA (cf. Figs. 2(a) and IV-E). These cross-domain errors are particularly severe when measurement changes are significant across domains due to variations in the domain parameter.

To quantify domain similarity, we compute the cosine similarities among the vectors $\{\mathbf{c}_j\}_{j=1}^3$. Let $\rho_{i,j}$ denote the similarity between \mathbf{c}_i and \mathbf{c}_j . For the structured and random gain experiments, the similarity values are $\{\rho_{1,2}, \rho_{2,3}, \rho_{3,1}\} = \{0.73, 0.76, 0.99\}$ and $\{0.59, 0.78, 0.82\}$, respectively. Due to the high similarity between domains 1 and 3 in the structured gain case ($\rho_{1,3} = 0.99$), the NMSE degradation when testing PT-D1 on D3 and vice versa is limited to around 5 dB. In contrast, for less similar pairs—for example, testing PT-D2 on D3—the NMSE degradation exceeds 20 dB.

Comparing the proposed P-TDA and DD-TDA methods to PT, we find that the NMSE and HR values remain consistent across domains. These results demonstrate that a single network can adapt to multiple domains, eliminating the need to train separate networks for each one.

B. Generalization

To assess the domain generalization capability of the proposed approaches for the calibration problem, we trained the models on 45 different domains (D1-D45) and then tested them on five unseen domains (D46-D50). For the JT, P-TDA, and DD-TDA methods, we generated $N = 10,000$ examples from each domain, which amounts to a total of 500,000 examples for training and testing. Whereas, for the PT models, we generated 50000 examples per domain. The datasets were divided into test, validation, and train sets in proportions of 10%, 20%, and 70%, respectively. In all these cases, the gains were generated as in 25.

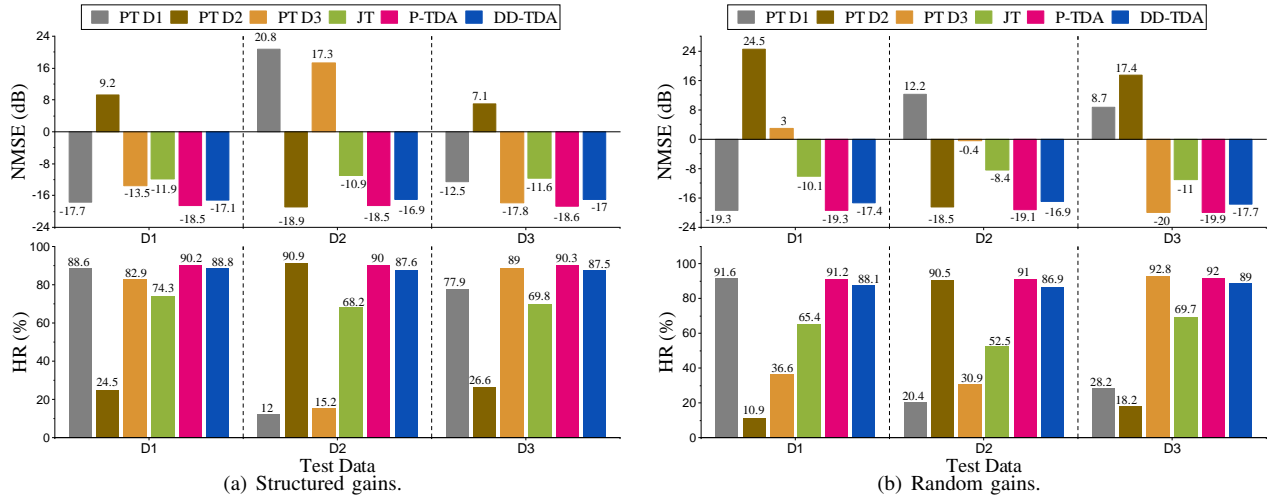


Fig. 11. Comparison of the proposed methods with the JT and PT methods for the sparse gain calibration problem. The P-TDA/DD-TDA has comparable performance to PT, demonstrating the domain-adaptability aspect.

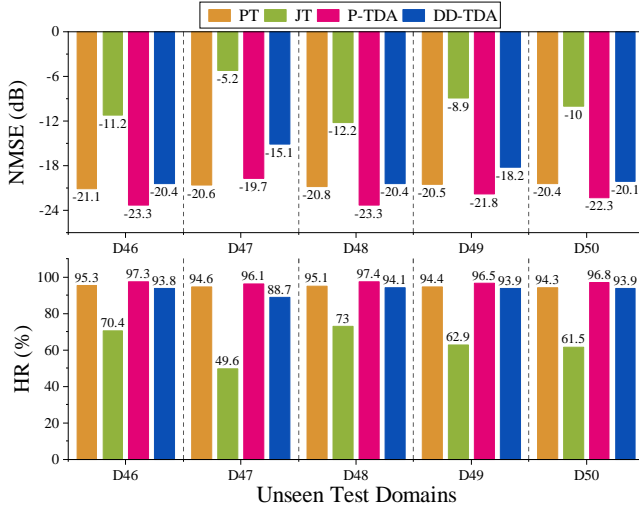


Fig. 12. Generalization performance of models, across domains with structured calibration gains. The JT, P-TDA, and DD-TDA models were trained on 45 domains and tested on 5 unseen domains.

The NMSEs and HRs, for the JT and PT methods, together with P-TDA and DD-TDA, are shown in Fig. 12. We note that for all the unseen domains, the NMSEs in the PT approaches are 8-15 dB lower than the JT methods. Both the P-TDA and DD-TDA methods result in 10-13 dB lower NMSEs compared to the JT methods. Comparing the P-TDA and the PT methods, we note that the NMSEs of the P-TDA approach are within a ± 3 dB range of the corresponding PT error for all the unseen domains. Similarly, the HRs of P-TDAs are within $\pm 4\%$ of those of the PT. This shows the generalization ability of the proposed networks.

Next, we consider a non-linear inverse problem of phase retrieval for P-TDA and DD-TDA methods.

VI. DOMAIN ADAPTIVE PHASE RETRIEVAL ALGORITHM

We next demonstrate the proposed tunable domain adaptation framework on the sparse phase retrieval (PR) problem [47], [48], [49]. Specifically, the measurements are modeled as

$$\mathbf{y} = |\mathbf{A}\mathbf{x}|^2 + \boldsymbol{\eta}, \quad \boldsymbol{\eta} \sim \mathcal{N}(\mathbf{0}, \sigma^2 \mathbf{I}_{N_y}), \quad (26)$$

where $\mathbf{y} \in \mathbb{R}^{N_y}$, $\mathbf{x} \in \mathbb{R}^{N_x}$, $\mathbf{A} \in \mathbb{R}^{N_y \times N_x}$ with $\|\mathbf{x}\|_0 = L$, and $\boldsymbol{\eta} \in \mathbb{R}^{N_y}$ is Gaussian noise. Unlike the linear settings considered earlier, here only the magnitudes of the measurements are observed. The goal is to estimate \mathbf{x} (up to a global phase), which makes the measurements a nonlinear function of \mathbf{x} . We show that a variant of LISTA can not be applied in this case.

Conventional sparse PR algorithms typically assume that the sparsity level L is known. If L changes, both traditional algorithms [47], [49] and their unrolled counterparts [48] may fail. Hence, we consider the sparsity L as the domain parameter, that is, $\theta = L$. In what follows, we first review an unrolled solution to the PR problem used for PT and JT, then identify the tunable parameter β , and finally describe the design of g_φ and h_φ for P-TDA and DD-TDA.

A. Phase Retrieval Algorithm

We build on the sparse-PR algorithm proposed in [49], which consists of two stages. The first stage estimates the support of \mathbf{x} by minimizing $C_A(\mathbf{x}) = \frac{1}{2N_y} \|\mathbf{z} - |\mathbf{A}\mathbf{x}|\|_2^2$, where \mathbf{z} is the elementwise square-root of \mathbf{y} . At the $(k+1)$ -th iteration, the support is estimated as

$$S_{k+1} = \text{supp}(\mathcal{H}_L(\mathbf{x}^k - \alpha_{1,k} \nabla C_A(\mathbf{x}^k))), \quad (27)$$

where $S_{k+1} \subset \{1, 2, \dots, N_x\}$ with $|S_{k+1}| = L$ and ∇C_A is the gradient of $C_A(\mathbf{x})$. Here, $\mathcal{H}_L(\mathbf{x})$ selects the L largest elements of \mathbf{x} . In the second stage, the amplitudes at the estimated support are refined as

$$\mathbf{x}^{k+1}(S_{k+1}) = \mathbf{x}^{k+1}(S_{k+1}) - \alpha_{2,k} \mathbf{p}^k(S_{k+1}), \quad (28)$$

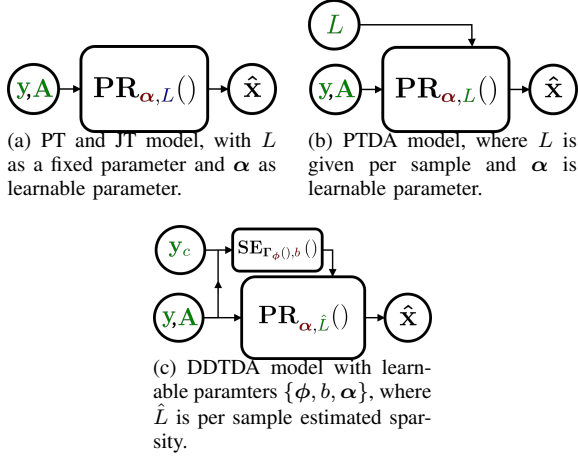


Fig. 13. $\text{PR}_{\alpha, L}(\cdot)$ is the tunable model for sparse phase retrieval. Note: Green symbols represent the data available at inference time. Red symbols are trainable parameters, and blue symbols are fixed parameters.

where $\mathbf{p}^k(S_{k+1})$ is computed using the gradient and Hessian of $\frac{1}{4N_y} \|\mathbf{y} - |\mathbf{A}\mathbf{x}|^2\|_2^2$ at \mathbf{x}_k (cf. [49]). In the updates (27) and (28), $\alpha = [\alpha_1 \ \alpha_2]$ are the step sizes.

B. Unfolding and Learnable/Tunable Parameters

Unfolding this algorithm yields a K -layer PR network that estimates \mathbf{x} as $f_{\alpha, \beta}(\mathbf{y})$. In the unfolding, we learn $\alpha = [\alpha_1 \ \alpha_2] \in \mathbb{R}^{K \times 2}$, while gradients and Hessians depend only on \mathbf{A} and \mathbf{x}_k . In this unfolding, we learn α while updating the gradients/Hessians using \mathbf{A} and the previous-layer's estimate. Importantly, we set $\beta = L = \theta$.

Unlike NA-LISTA and gain calibration, where β had no direct interpretation, here β is precisely the sparsity level. Thus, in PT and JT, we set $\beta = L$; in P-TDA, $g_\varphi(\theta) = \theta$, with no additional learning. Hence, PT, JT, and P-TDA all assume known sparsity. Next, we consider sparsity estimation for DD-TDA.

C. Sparsity Estimation for DD-TDA

Estimating sparsity from compressed measurements is challenging, particularly in the presence of noise [50], [51]. Existing methods often rely on specially designed sensing matrices, such as Gaussian/Cauchy [50] or binary constructions [51]. The PR setting is even more difficult since only magnitude measurements are available.

We adapt the approach of [50] to PR. Consider an auxiliary measurement $\mathbf{y}_c = |\mathbf{A}_c \mathbf{x}|^2 + \eta_c$, where \mathbf{A}_c is drawn from a Cauchy distribution, while \mathbf{A} in (26) is Gaussian. The sparsity can then be estimated as $\left[\hat{T}_1^2(\mathbf{y}_c) / \hat{T}_2^2(\mathbf{y}) \right]$, where

$$\hat{T}_1(\mathbf{y}_c) = \frac{\text{median}(\sqrt{|\mathbf{y}_c|})}{\gamma_c}, \quad \text{and} \quad \hat{T}_2^2(\mathbf{y}) = \frac{\|\sqrt{\mathbf{y}}\|_2^2}{N_y \gamma_g^2}, \quad (29)$$

with γ_c, γ_g depending on the respective distributions and not requiring precise knowledge in practice.

Building on this, we define a sparsity estimator (SE) as

$$\begin{aligned} \text{SE}_{[\gamma_c, \gamma_g, b]}(\mathbf{y}, \mathbf{y}_c) &= \left[\frac{\hat{T}_1^2(\mathbf{y}_c)}{\hat{T}_2^2(\mathbf{y})} + b \right] \\ &= N_y \left[\frac{(\text{median}(\sqrt{|\mathbf{y}_c|}))^2 \gamma_g^2}{\|\sqrt{\mathbf{y}}\|_2^2 \gamma_c^2} + b \right], \quad (30) \end{aligned}$$

where the bias term b compensates for estimation errors. The parameters $[\gamma_c, \gamma_g]$, related to the data distribution, are estimated from $[\mathbf{y}, \mathbf{y}_c]$ using a neural network $\Gamma_\phi(\mathbf{y}, \mathbf{y}_c)$ with trainable parameters ϕ . Hence, the tunable parameter estimator for this problem is given by $h_\varphi(\mathbf{y}, \mathbf{y}_c) = \text{SE}_{[\Gamma_\phi(\mathbf{y}, \mathbf{y}_c), b]}(\mathbf{y}, \mathbf{y}_c)$, where the learnable parameters are $\varphi = [\phi, b]$.

Compared to PT, JT, and P-TDA, the DD-TDA method requires N_c additional measurements due to estimator limitations. A better sparsity estimator could avoid the extra measurements. Further, unlike in earlier applications where β lacked a direct physical interpretation, here, β corresponds to the sparsity level and thus has ground-truth during training. As a result, h_φ can be trained independently of the PR module.

The architectures for the different methods for the PR problem are shown in Fig 13.

D. Results and Discussion

To evaluate the performance of the proposed adaptive phase retrieval framework, we conduct a series of experiments comparing the P-TDA and DD-TDA models against the PT and JT baselines. The domain parameter is the sparsity level L of the signal \mathbf{x} .

Data Generation and Network Architecture: We generated a synthetic dataset according to the measurement model in (26). The measurement matrix $\mathbf{A} \in \mathbb{R}^{N_y \times N_x}$ was constructed with entries drawn from a standard Gaussian distribution, i.e., $\mathbf{A}_{:j} \sim \mathcal{N}(0, \gamma \mathbf{I}_{N_y})$. For the DD-TDA model, an additional measurement matrix $\mathbf{A}_c \in \mathbb{R}^{N_{y_c} \times N_x}$ was used for sparsity estimation, with its entries drawn from a standard Cauchy distribution. The non-zero entries of the ground truth sparse signal $\mathbf{x} \in \mathbb{R}^{N_x}$ are chosen randomly from the set $\{+1, -1\}$.

The experiments were conducted across three distinct domains defined by their sparsity levels: D1 ($L = 10$), D2 ($L = 7$), and D3 ($L = 4$). We set the signal and measurement dimensions as $N_x = 1700$, $N_y = 1200$, and $N_{y_c} = 400$. A total of $N = 6000$ samples were generated, which were then split into 80% training, 15% validation, and the remaining 5% as testing sets.

For the PT approach, three separate models (PT D1, PT D2, PT D3) were trained exclusively on data corresponding to their respective sparsity domains. In contrast, the JT, P-TDA, and DD-TDA models were all trained on a mixed dataset containing samples from all three domains. The unfolded PR network for all models consists of $K = 10$ layers, with the step sizes α_1 and α_2 as learnable parameters. The key tunable parameter is the sparsity level $\beta = L$ used in the hard-thresholding operator $\mathcal{H}_L(\cdot)$ within each layer. For P-TDA, this parameter is set to the known ground-truth sparsity for each sample.

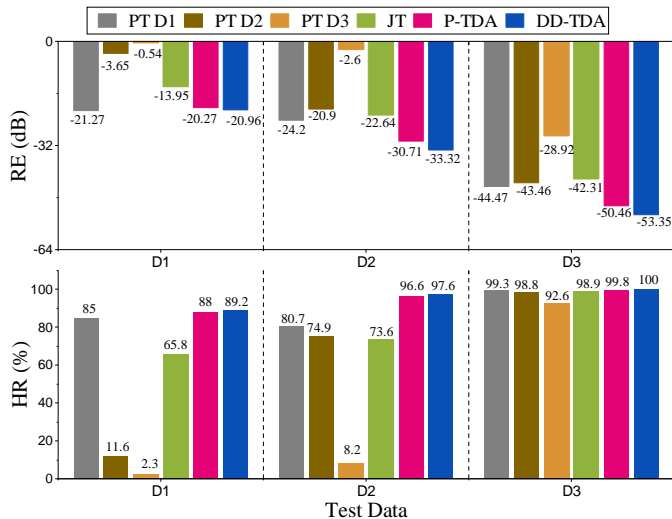


Fig. 14. Comparison of the proposed methods with the JT and PT methods for Phase Retrieval with sparsity [10, 7, 4] and HR tol: 0.05.

For DD-TDA, the sparsity is estimated by the network $SE_{[\Gamma_\phi(\cdot), b]}(\cdot)$ where the function Γ_ϕ comprises two layers of multi-layer perceptrons. This network is learned first in a separate training stage. Subsequently, these parameters are frozen, and the PR network is integrated into the DD-TDA model, where only $\alpha = [\alpha_1, \alpha_2]$ is trained.

Performance Metrics: Model performance was evaluated using two primary metrics, Relative Error (RE) and HR. Given the global phase ambiguity inherent in phase retrieval, the RE between a ground truth signal \mathbf{x}^* and an estimate $\hat{\mathbf{x}}$ is defined to account for potential sign flips as,

$$RE(\hat{\mathbf{x}}, \mathbf{x}^*) = \min \left(\frac{\|\hat{\mathbf{x}} - \mathbf{x}^*\|_2}{\|\mathbf{x}^*\|_2}, \frac{\|\hat{\mathbf{x}} + \mathbf{x}^*\|_2}{\|\mathbf{x}^*\|_2} \right). \quad (31)$$

The RE is reported in decibels (dB). The HR measures the fraction of correctly identified non-zero elements in the support of \mathbf{x}^* whose estimated amplitudes are within a specified tolerance. For our experiments, the tolerance for HR was set to $t = 0.05$.

Comparison of Methods: The performance of the different models on the three test domains is presented in Fig. 14. The results clearly demonstrate the of fixed-parameter models and the advantages of our proposed adaptive approaches.

The PT models, designed as domain specialists, perform well only when the test domain matches their training domain. For instance, PT D3, trained with $L = 4$, achieves a low RE on D3 test data but fails catastrophically on D1 ($L = 10$) and D2 ($L = 7$). This is because its $\mathcal{H}_L(\cdot)$ operator is fixed to select only four components, making it impossible to recover signals with higher sparsity. Conversely, PT D1 is trained with $L = 10$. When tested on D2 and D3, its operator selects the 10 largest components, which are sufficient to contain the true supports of size seven and four, respectively. This leads to surprisingly robust performance across all domains, although its performance on D1 is not as strong as the adaptive models, indicating that simply over-fixing the sparsity parameter is a suboptimal strategy. The JT model, trained on a mix of all domains by setting $L = 10$, finds a middle ground and delivers

TABLE V
COMPARISON OF DD-TDA WITH AND WITHOUT CAUCHY MEASUREMENTS FOR PHASE RETRIEVAL

K	Metric	DD-TDA	DD-TDA _{Base}
10	NMSE (dB)	-20.96	-1.91
	HR (%)	89.2	33.1
7	NMSE (dB)	-41.23	-30.41
	HR (%)	97.6	98.0
4	NMSE (dB)	-52.14	-44.88
	HR (%)	100.0	100.0

average performance across all the domains, failing to match the PT models in their respective domains.

In sharp contrast, both the P-TDA and DD-TDA models exhibit consistently superior performance across all test domains, achieving the lowest RE and highest HR values. This accomplishment is directly related to their capacity to dynamically adjust the sparsity parameter L on a per-sample basis. The P-TDA model, which uses the ground-truth sparsity, sets a high-performance benchmark. The DD-TDA model estimates the sparsity directly from the measurements, performing on par with, and in some cases even slightly better than, the P-TDA model. This performance advantage is due to the learned bias term b in the sparsity estimation network $h_\varphi(\cdot)$. This bias allows the model to learn to slightly overestimate the sparsity, a strategy which can be beneficial in noisy conditions by preventing the premature discarding of true signal components.

DD-TDA Without Cauchy Measurements: To evaluate the necessity of auxiliary Cauchy measurements for sparsity estimation in DD-TDA, we conducted a study comparing the full DD-TDA method with a baseline variant that operates without Cauchy measurements. The baseline DD-TDA (DD-TDA_{Base}) uses only the standard Gaussian measurements \mathbf{y} to estimate sparsity through the neural network $h_\varphi(\mathbf{y})$, removing the explicit sparsity estimator $SE(\cdot)$ from Eq. 30 with a light weight MLP.

As shown in Table V, the DD-TDA_{Base} achieves reasonable performance without auxiliary measurements, particularly for lower sparsity levels. For $K = 7$ and $K = 4$, the method achieves NMSE values of -30.41 dB and -44.88 dB with near-perfect hit rates of 98.0% and 100.0%, respectively, closely matching the performance of DD-TDA with Cauchy measurements. However, performance degrades significantly at higher sparsity like for $K = 10$, where NMSE drops to -1.91 dB and HR falls to 33.1%, compared to -20.96 dB and 89.2% with Cauchy measurements.

This demonstrates a clear trade off in the design choice. For applications with low to moderate sparsity levels, the baseline DD-TDA can operate effectively using only standard Gaussian measurements, avoiding the need for additional sensing protocols. However, for high-sparsity scenarios, the auxiliary Cauchy measurements provide substantial performance gains by enabling more accurate sparsity estimation, which is critical when phase information is unavailable.

Overall, the results confirm that adapting the sparsity parameter is crucial for robust phase retrieval across varying domains. The proposed DD-TDA framework provides an effective, data-driven mechanism to achieve this adaptation, yielding a single model that outperforms generalist baselines.

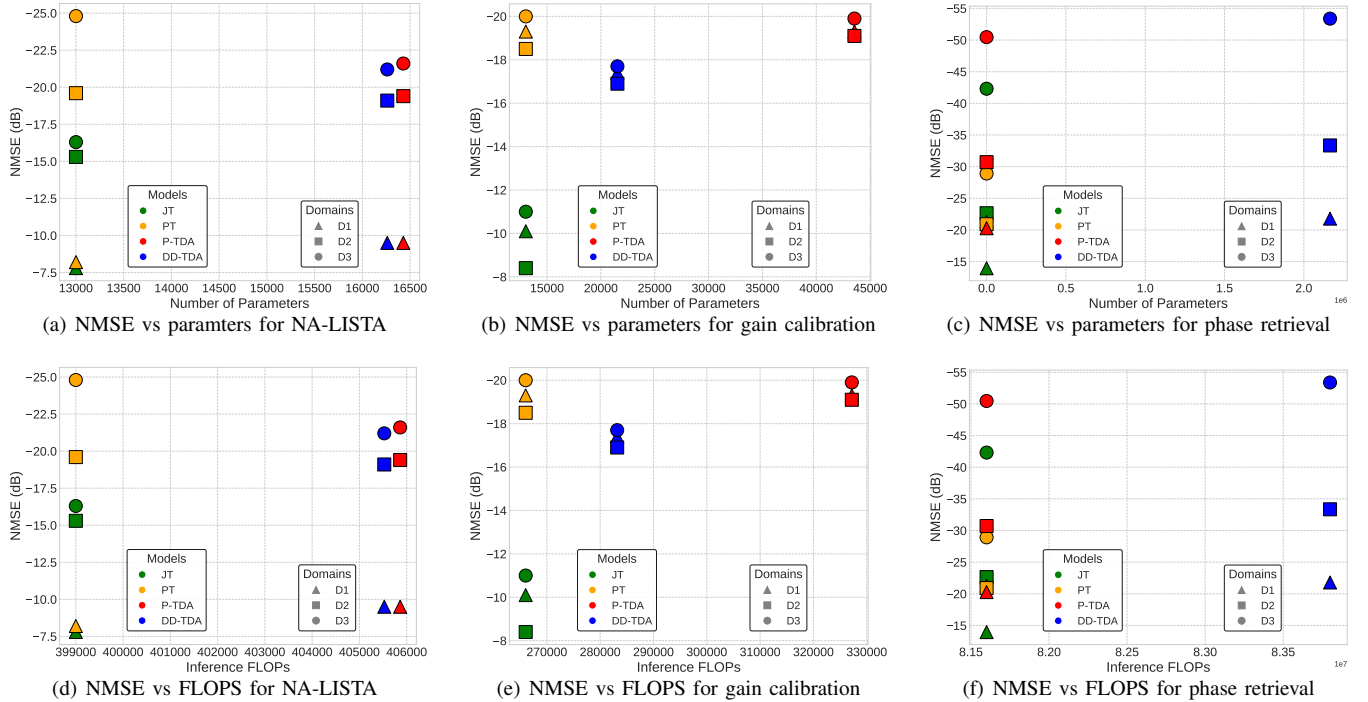


Fig. 15. A comparison of NMSE against the number of parameters and FLOPS for different methods.

VII. NETWORK COMPLEXITY AND PERFORMANCE COMPARISONS

In all the three inverse problems, additional networks g_φ and h_φ are added to P-TDA and DD-TDA methods, respectively. This results in additional parameters and computations in P-TDA and DD-TDA in comparison to the PT and JT methods, as compared in Fig. 15. The plots show that the P-TDA/DD-TDA methods require considerably higher numbers of parameters and FLOPS. However, we would like to mention that the networks g_φ and h_φ were intentionally implemented in a non-optimized form, as the focus of this work was to demonstrate the feasibility of tunable adaptation. Their parameter footprint can be greatly reduced in practice without modifying the underlying methodology. Further, note that PT requires training and storing a separate LISTA model for each domain. Thus, the parameter/FLOP count grows linearly with the number of domains. In contrast, DD-TDA uses one model trained on mixed data and can generalize to new domains without access to the domain labels or parameters.

It is also worth noting from Figs. 15(c) and 15(f) that for the phase retrieval problem, the P-TDA model exhibits a parameter count comparable to the PT and JT methods. However, there is a significant increase in the number of parameters for the DD-TDA model. This jump is because of the architecture of the tuning function, $\Gamma(\cdot)$. In our implementation, $\Gamma(\cdot)$ is a two-layer network that maps a high-dimensional input of size 1600 to an output of size 10×2 . The high input dimension of this network is the main reason for the large parameter footprint. This particular component offers a clear opportunity for optimization, and its architecture could be redesigned to create a more lightweight network, thereby

reducing the overall complexity of the DD-TDA model.

VIII. CONCLUSION

In this paper, we propose a systematic framework for interpretable, unrolled architecture-based domain-adaptive sparse signal recovery with two tunability strategies: P-TDA, which uses known domain parameters, and DD-TDA, which derives domain-relevant variations from the data itself. We concentrate on three realistic and different types of domain variability: additive noise variance, sensor calibration gains, and sparse phase retrieval across domains.

In the case of noise-varying domains, our approaches enable the sparse recovery network to adjust its thresholding behavior without requiring domain-specific retraining. We show that P-TDA can successfully normalize the input using known gains in the more difficult blind calibration scenario. When measurements are affected by unknown gain vectors, DD-TDA learns to correct for gain distortions without explicit access to the calibration parameters. We further demonstrated the framework’s versatility on the challenging problem of sparse phase retrieval, where our DD-TDA model successfully adapted to varying signal sparsity levels using a data-driven estimator. Across all applications, the suggested approaches consistently exceeded normal JT models and closely resembled or matched the performance of domain-specific PT models. In the future, unsupervised domain learning will be used to extend this framework to incorporate more complex models.

REFERENCES

- [1] J. Yosinski, J. Clune, Y. Bengio, and H. Lipson, “How transferable are features in deep neural networks?” in *Proc. Adv. Neural Info. Process. Sys. (NeurIPS)*, 2014, pp. 3320–3328.

- [2] K. He, X. Zhang, S. Ren, and J. Sun, "Deep residual learning for image recognition," in *Proc. IEEE Int. Conf. Comput. Vision and Pattern Recognition (CVPR)*, 2016, pp. 770–778.
- [3] J. Devlin, M.-W. Chang, K. Lee, and K. Toutanova, "Bert: Pre-training of deep bidirectional transformers for language understanding," in *Proc. North American Chap. Asso. Comput. Linguistics (NAACL-HLT)*, 2019, pp. 4171–4186.
- [4] S. J. Pan and Q. Yang, "A survey on transfer learning," *IEEE Trans. Knowl. Data Eng.*, vol. 22, no. 10, pp. 1345–1359, 2010.
- [5] H.-H. Tseng, H.-Y. Lin, K.-H. Hung, and Y. Tsao, "Interpretations of domain adaptations via layer variational analysis," *arXiv preprint arXiv:2302.01798*, 2023.
- [6] Y. He, H. Wang, B. Li, and H. Zhao, "Gradual domain adaptation: Theory and algorithms," *J Machine Learning Res.*, vol. 25, no. 361, pp. 1–40, 2024.
- [7] A. Farahani, S. Voghoei, K. Rasheed, and H. R. Arabnia, "A brief review of domain adaptation," in *Proc. Adv. Data Sci. Info. Engg.* Cham: Springer International Publishing, 2021, pp. 877–894.
- [8] A. Singh and S. Chakraborty, "Deep domain adaptation for regression," in *Development and Analysis of Deep Learning Architectures*. Springer, 2019, pp. 91–115.
- [9] D. Obst, B. Ghattas, J. Cugliari, G. Oppenheim, S. Claudel, and Y. Goude, "Transfer learning for linear regression: A statistical test of gain," *arXiv preprint arXiv:2102.09504*, 2021.
- [10] S. Li, T. T. Cai, and H. Li, "Transfer learning for high-dimensional linear regression: Prediction, estimation and minimax optimality," *J. Royal Stat. Society Series B: Statistical Methodology*, vol. 84, no. 1, pp. 149–173, 2022.
- [11] W. Mao, K. Liu, Y. Zhang, X. Liang, and Z. Wang, "Self-supervised deep tensor domain-adversarial regression adaptation for online remaining useful life prediction across machines," *IEEE Trans. Inst. Meas.*, vol. 72, pp. 1–16, 2023.
- [12] V. Monga, Y. Li, and Y. C. Eldar, "Algorithm unrolling: Interpretable, efficient deep learning for signal and image processing," *IEEE Mag. Signal Processing*, vol. 38, no. 2, pp. 18–44, 2021.
- [13] D. Donoho, "Compressed sensing," *IEEE Trans. Inf. Theory*, vol. 52, no. 4, pp. 1289–1306, 2006.
- [14] I. Daubechies, M. Defrise, and C. De Mol, "An iterative thresholding algorithm for linear inverse problems with a sparsity constraint," *Commun. Pure Applied Math.*, vol. 57, no. 11, pp. 1413–1457, 2004.
- [15] K. Gregor and Y. LeCun, "Learning fast approximations of sparse coding," in *Proc. Int. Conf. Machine Learn. (ICML)*, 2010, pp. 399–406.
- [16] D. L. Donoho and I. M. Johnstone, "Ideal spatial adaptation by wavelet shrinkage," *Biometrika*, vol. 81, no. 3, pp. 425–455, 1994.
- [17] Y. Guo, H. Shi, A. Kumar, K. Grauman, T. Rosing, and R. Feris, "Spot-tune: transfer learning through adaptive fine-tuning," in *Proceedings of the IEEE/CVF conference on computer vision and pattern recognition*, 2019, pp. 4805–4814.
- [18] M. Long, J. Wang, G. Ding, J. Sun, and P. S. Yu, "Transfer feature learning with joint distribution adaptation," in *Proc. Int. Conf. Computer Vision (ICCV)*, 2013, pp. 2200–2207.
- [19] M. Long, Y. Cao, J. Wang, and M. I. Jordan, "Learning transferable features with deep adaptation networks," in *Proc. Int. Conf. on Machine Learning (ICML)*, 2015, pp. 97–105.
- [20] E. Tzeng, J. Hoffman, N. Zhang, K. Saenko, and T. Darrell, "Deep domain confusion: Maximizing for domain invariance," *arXiv preprint arXiv:1412.3474*, 2014.
- [21] S. Motiian, M. Piccirilli, D. A. Adjeroh, and G. Doretto, "Unified deep supervised domain adaptation and generalization," in *Proc. Int. Conf. Computer Vision (ICCV)*, 2017, pp. 5715–5725.
- [22] B. Tolooshams, X. Wang, X. He, Y. Zhang, and M. Jacob, "Transfer learning for linear regression: A statistical test of gain," in *arXiv preprint arXiv:2102.09504*, 2021.
- [23] Y. Lu, J. Qin, and Y. Wang, "Deep domain adaptation for regression," in *Proc. Int. Conf. Machine Learning (ICML)*, 2019, pp. 97–105.
- [24] H. Li, Y. Wang, and X. Xie, "Transfer learning for high-dimensional linear regression: Prediction via information borrowing," *J. Royal Statistical Soc.: Series B*, vol. 84, no. 1, pp. 149–175, 2023.
- [25] Y. Zhang, X. Wang, and X. He, "Representation transfer learning for semiparametric regression," *arXiv preprint arXiv:2406.13197*, 2024.
- [26] W. Chen, Y. Li, and Y. Zhou, "Self-supervised deep domain-adversarial regression adaptation for remaining useful life prediction," in *IEEE Trans. Ind. Electron.*, 2022, p. 9769904.
- [27] D. Pardoe and P. Stone, "Boosting for regression transfer," in *Proc. Int. Conf. on Machine Learning (ICML)*, 2010, pp. 863–870.
- [28] S. H. Chan, "Algorithm-induced prior for image restoration," *arXiv preprint arXiv:1602.00715*, 2016.
- [29] A. Beck and M. Teboulle, "A fast iterative shrinkage-thresholding algorithm with application to wavelet-based image deblurring," in *Proc. IEEE Int. Conf. Acoust., Speech, and Signal Process. (ICASSP)*, 2009, pp. 693–696.
- [30] A. Aberdam, A. Golts, and M. Elad, "Ada-lista: Learned solvers adaptive to varying models," *IEEE Trans. Pattern Anal. Mach. Intell.*, vol. 44, no. 12, pp. 9222–9235, 2021.
- [31] X. Chen, J. Liu, Z. Wang, and W. Yin, "Theoretical linear convergence of unfolded ISTA and its practical weights and thresholds," *Adv. Neural Info. Process. Syst.*, vol. 31, 2018.
- [32] J. Liu and X. Chen, "ALISTA: Analytic weights are as good as learned weights in LISTA," in *Int. Conf. Learning Representations (ICLR)*, 2019.
- [33] X. Chen, J. Liu, Z. Wang, and W. Yin, "Hyperparameter tuning is all you need for LISTA," *Adv. Neural Info. Process. Syst.*, vol. 34, pp. 11 678–11 689, 2021.
- [34] Z. Li, K. Wu, Y. Guo, and C. Zhang, "Learned ISTA with error-based thresholding for adaptive sparse coding," in *Int. Conf. Acoust. Speech Signal Process. (ICASSP)*. IEEE, 2024, pp. 9301–9305.
- [35] N. P. Galatsanos and A. K. Katsaggelos, "Methods for choosing the regularization parameter and estimating the noise variance in image restoration and their relation," *IEEE Trans. Image Process.*, vol. 1, no. 3, pp. 322–336, 1992.
- [36] C. Liu, R. Szeliski, S. B. Kang, C. L. Zitnick, and W. T. Freeman, "Automatic estimation and removal of noise from a single image," *IEEE Trans. Pattern Anal. Mach. Intell.*, vol. 30, no. 2, pp. 299–314, 2008.
- [37] X. Liu, M. Tanaka, and M. Okutomi, "Noise level estimation using weak textured patches of a single noisy image," in *Int. Conf. Image Process. IEEE*, 2012, pp. 665–668.
- [38] G. H. Golub, M. Heath, and G. Wahba, "Generalized cross-validation as a method for choosing a good ridge parameter," *Technometrics*, vol. 21, no. 2, pp. 215–223, 1979.
- [39] Y. Kvich, P. Reshma, P. Pradhan, R. Randhi, and Y. C. Eldar, "Deep unfolding of tail-based methods for robust sparse recovery under noise and model mismatch," *IEEE Trans. on Neural Networks and Learning Systems*, 2025.
- [40] J. Song, C. Meng, and S. Ermon, "Denoising diffusion implicit models," *arXiv preprint arXiv:2010.02502*, 2020.
- [41] A. Jhwar, "Mnist handwritten digit classifier (handwritten-digit-recognition)," <https://github.com/aakashjhwar/handwritten-digit-recognition>, 2018, GitHub repository.
- [42] O. Steiger, J. Felder, and S. Weiss, "Calibration of time-of-flight range imaging cameras," in *Proc. Int. Conf. on Image Process.* IEEE, 2008, pp. 1968–1971.
- [43] S. Mersmann, A. Seitel, M. Erz, B. Jähne, F. Nickel, M. Mieth, A. Mehrabi, and L. Maier-Hein, "Calibration of time-of-flight cameras for accurate intraoperative surface reconstruction," *Medical Physics*, vol. 40, no. 8, p. 082701, 2013.
- [44] A. Paulraj and T. Kailath, "Direction of arrival estimation by eigenstructure methods with unknown sensor gain and phase," in *Proc. IEEE Int. Conf. Acoust., Speech, and Signal Process. (ICASSP)*, vol. 10, 1985, pp. 640–643.
- [45] C. Schulke, F. Caltagirone, F. Krzakala, and L. Zdeborová, "Blind calibration in compressed sensing using message passing algorithms," *Adv. Neural Info. Process. Syst.*, vol. 26, 2013.
- [46] B. Tolooshams, S. Mulleti, D. Ba, and Y. C. Eldar, "Unrolled compressed blind-deconvolution," *IEEE Trans. Signal Process.*, vol. 71, pp. 2118–2129, 2023.
- [47] G. Wang, L. Zhang, G. B. Giannakis, M. Akçakaya, and J. Chen, "Sparse phase retrieval via truncated amplitude flow," *IEEE Transactions on Signal Processing*, vol. 66, no. 2, pp. 479–491, 2017.
- [48] N. Naimipour, S. Khobahi, M. Soltanalian, H. Safavi, and H. C. Shaw, "Unfolded algorithms for deep phase retrieval," *Algorithms*, vol. 17, no. 12, p. 587, 2024.
- [49] J. F. CAI, Y. Long, R. WEN, and J. Ying, "A fast and provable algorithm for sparse phase retrieval," in *The Twelfth International Conference on Learning Representations*, 2024.
- [50] M. Lopes, "Estimating unknown sparsity in compressed sensing," in *International Conference on Machine Learning*. PMLR, 2013, pp. 217–225.
- [51] S. Thirupathirajan, S. Sreelal, B. Manoj *et al.*, "Sparsity order estimation for compressed sensing system using sparse binary sensing matrix," *IEEE Access*, vol. 10, pp. 33 370–33 392, 2022.